

AD-A053 351

AIR FORCE INST OF TECH WRIGHT-PATTERSON AFB OHIO SCH--ETC F/G 20/5
SPATIAL AND TEMPORAL CODING OF GAAS LASERS FOR A LASER LINE SCA--ETC(U)
DEC 77 R S SHINKLE

UNCLASSIFIED

AFIT/GE0/EE/77-5

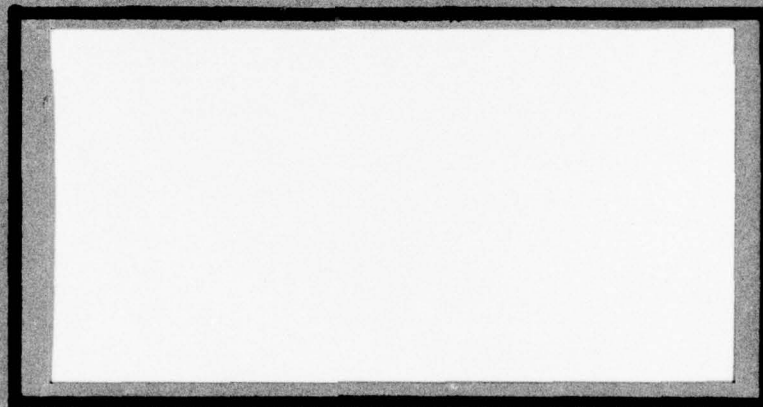
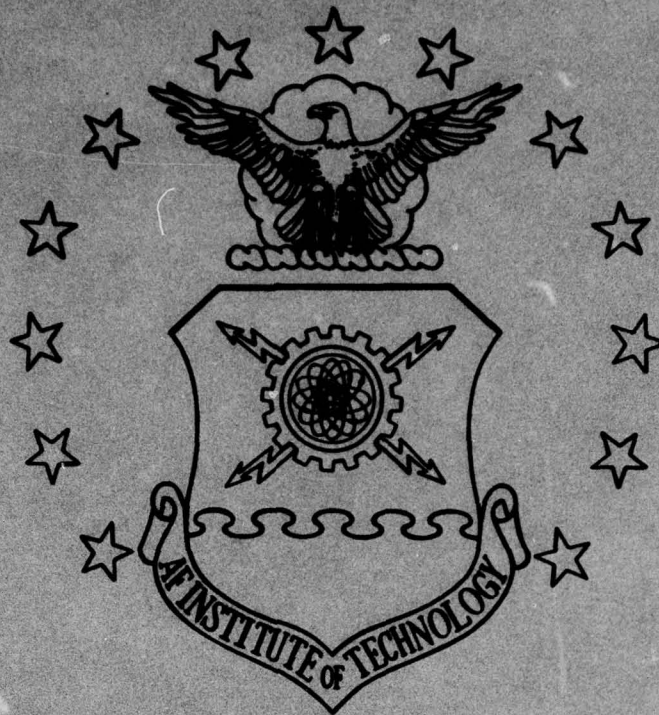
NL

1 of 2
AD
A053351



AD A053351

AD No. _____
DDC FILE COPY



UNITED STATES AIR FORCE
AIR UNIVERSITY
AIR FORCE INSTITUTE OF TECHNOLOGY
Wright-Patterson Air Force Base, Ohio



DISTRIBUTION STATEMENT A
Approved for public release;
Distribution Unlimited

(1)

AD A053351

AD No.
 DDC FILE COPY

SPATIAL AND TEMPORAL CODING OF GaAs
LASERS FOR A LASER LINE SCAN SENSOR
THESIS

GEO/EE/77-5

Reese S. Shinkle
Capt USAF

DDC
RECEIVED
MAY 2 1978
A

Approved for public release; distribution unlimited

6 SPATIAL AND TEMPORAL CODING OF GaAs LASERS FOR A LASER LINE SCAN SENSOR.

14 AFIT/GEO/EE/77-5

9 master's THESIS •

Presented to the Faculty of the School of Engineering
of the Air Force Institute of Technology

Air University

in Partial Fulfillment of the

Requirements for the Degree of Master of Science

123 p.

by

① Reese S. Shinkle B. E. E.
Capt USAF

Graduate Electro-Optics

11 Dec 1977

ACCESSION NO.

FILE

SERIAL

DATE

TIME

BY

REMARKS

CLASSIFICATION CODES

STATUS OF SPECIAL

Approved for public release; distribution unlimited.

Φ 12 225

Preface

This thesis was accomplished under the sponsorship of the Air Force Avionics Laboratory at Wright-Patterson Air Force Base, Ohio. It is an engineering study to determine the theoretically best combination of scan configuration and temporal intensity modulation in order to use N GaAs semiconductor laser sources to measure range and reflectance with a line scan system. Although it is basically a theoretical study, several practical implementation issues are also discussed.

I would like to express my appreciation to Mr. W. C. Schoonover of the Avionics Laboratory for the office space and support provided during the course of this study. I would also like to thank Dr. B. L. Sowers of the Avionics Laboratory for providing many helpful comments. I am grateful to fellow classmates Capts J. B. Armor, H. E. Hagemeyer, B. W. Lyons, and W. D. Strautman for the many helpful skill sessions. In addition, a sincere thank you also goes to Capt S. R. Robinson for the support and guidance he has provided during this nine-month period. Finally, special thanks go to my wife, Janice, whose patience and understanding during this period have contributed immeasurably to this final product.

Reese S. Shinkle

Contents

	Page
Preface	ii
List of Figures	v
List of Tables.	vii
List of Abbreviations and Symbols.	viii
Abstract	xiv
I. Introduction	1
Problem	3
Scope and Assumptions	4
Thesis Overview	5
II. Theoretical Background	6
Direct Detector Statistical Model	6
Parameter Estimation and Performance Theory	12
Additional Comments on Implementation	25
III. Spatial and Temporal Coding Analysis	39
Introduction	39
N Sources in Parallel, Pulse Code Modulation	43
N Sources in Series, Pulse Code Modulation	49
N Sources in an Array, Pulse Code Modulation	51
N Sources in Parallel, Sinusoidal Modulation	53
N Sources in Parallel, Multiple Sinusoidal Modulation.	54
Temporal Modulation Via Electro-Optic Modulators	57
Temporal Modulation Via Spatial Coding	58
N Sources in Parallel, OOK Sinusoidal Modulation	61
q-Staring Sources and Detectors, Pulse Code Modulation.	67
q-Staring Sources and Detectors, Spatial and Temporal Modulation	69
N Overlapping Sources, Pulse Code Modulation	71

Contents

	Page
IV. Comparisons of the Various Spatial-Temporal Coding Combinations	74
Comparisons of the Pulse Code Modulation Class . . .	75
Comparisons of the Sinusoidal Modulation Class . . .	80
Comparisons of the Non-Scanning Class	83
Comparison of PCM and Sinusoidal Modulations	84
Comparison of PCM and OOK Sinusoidal Modulations . .	87
Comparison of q-PCM Channels and N-OOK Sinusoidal Modulated Channels	90
Comparisons Results - rms Power Limited Sources . .	93
V. Conclusions and Recommendations	95
Conclusions	95
Recommendations	98
Bibliography	100
Appendix A: Additive Noise Model for Direct Detection . . .	102
Vita	105

List of Figures

<u>Figure</u>		<u>Page</u>
1	Basic Geometry and Block Diagram of a Laser Line Scan Sensor	2
2	Direct Detector Noise Model	9
3	$m \times n$ Bank of Correlators Implementation of ML Estimators	16
4	Suboptimum ML Estimators	18
5	Matched Filter Implementation of ML Estimators	27
6	Matched Filter Response for a Single Pulse	27
7	Error Due to Large Sidelobes Plus a Noise Spike	28
8	Normalized Autocorrelation of PN Code p Chips Long. .	31
9	Autocorrelation of a Totally Orthogonal Complimentary Pair	32
10	ML Estimator for Phase	36
11	One Source Laser Line Scan System	42
12	N Sources in Parallel	43
13	Receiver Configuration for "Fast Parallel Scan-PN Code System	46
14	Receiver Configuration for CP Coding	48
15	N Sources in Series	50
16	Receiver Configuration for "Series Scan-PC Modulation	51
17	Multiple Sinusoid Transmitter Configuration	55

List of Figures

<u>Figure</u>		<u>Page</u>
18	N Series, Spatially Coded Sources	59
19	N Parallel, Spatially Coded Transmitter Beams	60
20	Hybrid Spatial-Temporal Code	61
21	On-Off-Keying Via Hybrid Spatial-Temporal Coding. . .	62
22	Transmitter Configuration for OOK.	63
23	Receiver Configuration for OOK Modulation	64
24	q-Staring Source-Detector Pairs	68
25	q-Staring Source-Detector Pairs, Spatially and Temporally Modulated	70
26	N Overlapping Transmitted Laser Beams	72
27	"Footprint" of N-Overlapping Beams Partitioned by N-Detector FOVs	73
28	Graph of $R_{amb} = \frac{\pi c}{4} t_o \left(\frac{\sigma_{r-s}}{\sigma_{r-PCM}} = 1 \right)$	87

List of Tables

<u>Table</u>		<u>Page</u>
1	Comparison of PCM Scan Characteristics	81
2	Spatial-Temporal Systems Characteristics	92

List of Abbreviations and Symbols

Abbreviations

BPF	bandpass filter
cm	centimeter
CP	Total Orthogonal Complimentary Pair Code
CW	Continuous Wave
db	decibel
DC	Direct Current
FOV	field-of-view
\ln	natural log
ML	Maximum likelihood
μm	micrometer
OOK	On-Off-Keyed
pdf	Probability density function
PCM	pulse code modulation
PLL	phase locked loop
PN	pseudo-noise code
rms	root mean square
SNR	signal-to-noise ratio

Symbols

A	"A" codeword of a complimentary pair
A_d	area of detector aperture
A_f	area on ground subtended by receiver field-of-view

List of Abbreviations and Symbols

Symbols	
A_R	area of receiver optics
B	"B" codeword of a complimentary pair
B_s^2	mean square bandwidth of signal $s(t)$
$B_{ U }^2$	mean square bandwidth of incident optical field
β	detector responsivity; average number of electrons generated per unit of incident optical energy
c	speed of light
E	expected value (ensemble average) operator
E_s	post detector signal energy for signal $s(t)$
E_{s-BPF}	signal energy of the bandpass filter detector output
$E_{s,\lambda}$	solar spectral irradiance
η	detector quantum efficiency
f	frequency
f_m	modulation frequency
f_o	optical frequency
$f_Z A$	probability density function Z given A
$F_s(f)$	Fourier transform of $s(t)$
h	Planck's constant
$h(t)$	Filter impulse response
$i(t)$	detector output current
i_b	background noise component of detector output current
i_D	dark current component of detector output current
i_{Th}	thermal noise component of detector output current

List of Abbreviations and Symbols

Symbols

J	matrix J
k	constant of proportionality
K	Boltzmann's constant
K_v	voltage controlled oscillator constant
$\lambda(t)$	detector rate function; events or electrons per second
λ_b	background noise rate function
λ_D	dark current rate function
λ_n	noise rate function ($\lambda_b + \lambda_D$)
λ_o	direct current component of $\lambda_s(t)$
$\Delta\lambda$	optical filter bandwidth
m	number of parallel sources in an $m \times n$ array
$m(t)$	intensity modulation impressed upon laser output
n	number of series sources in an $m \times n$ array
$n(t)$	additive noise
N	total number of scanning laser sources
$N(T)$	number of counts or events in the time interval $(0, T)$
$N_b(\tau_c)$	number of counts or events in the time interval $(0, \tau_c)$ due to background noise
$N_o/2$	two-sided noise power spectral density of a Gaussian random process
ω	radian frequency
p	number of chips in a pulse code modulation codeword

List of Abbreviations and Symbols

Symbols

P_d	signal power collected by the detector
P_t	power transmitted by the laser
q	the total number of pixels in a scan line
Q	a constant; the average number of counts over the observation interval
r	range
\hat{r}	range estimate
$R(\tau)$	autocorrelation
R_{amb}	maximum ambiguous range
R_{amb-CP}	maximum ambiguous range for a complimentary pair code
R_{amb-M}	maximum ambiguous range for Multiple Sinusoidal modulation
$R_{amb-PCM}$	maximum ambiguous range for pulse code modulation
R_{amb-PN}	maximum ambiguous range for pseudo-noise code
R_{amb-S}	maximum ambiguous range for a Single Sinusoidal
ρ	reflectance
$\hat{\rho}$	reflectance estimate
σ_r	range error standard deviation (root mean square error)
σ_{r-CP}	rms range error for a complimentary pair code
σ_{r-M}	rms range error for multiple sinusoidal modulation
$\sigma_{r-N-OOK}$	rms range error for N sources - OOK Sinusoidal modulation
σ_{r-OOK}	rms range error for OOK Sinusoidal Modulation

List of Abbreviations and Symbols

Symbols

$\sigma_{r\text{-PCM}}$	rms range error for pulse code modulation
$\sigma_{r\text{-PN}}$	rms range error for a pseudo-noise code
$\sigma_{r\text{-q-PN}}$	rms range error for q-Staring Sources-PCM
$\sigma_{\rho\text{-CP}}$	rms reflectance error standard deviation (root mean square error)
$\sigma_{\rho\text{-M}}$	rms reflectance error for complimentary pair code
$\sigma_{\rho\text{-N-OOK}}$	rms reflectance error for N-Sources-OOK sinusoidal Modulation
$\sigma_{\rho\text{-OOK}}$	rms reflectance error for OOK Sinusoidal Modulation
$\sigma_{\rho\text{-PCM}}$	rms reflectance error for pulse code modulation
$\sigma_{\rho\text{-PN}}$	rms reflectance error for pseudo-noise code
$\sigma_{\rho\text{-q-PCM}}$	rms reflectance error for q-Staring Source-PCM
$R_n(t, t')$	additive noise autocorrelation function
$s(t)$	intensity modulated optical signal
$S_n(f)$	double sided noise power spectral density
t	time
t_0	chip duration
t_r	transmission of receiver optics and atmospheric path
t_t	transmission of combined receiver optics and two-way atmospheric path
T	observation time interval
T_m	period of the modulation frequency f_m

List of Abbreviations and Symbols

Symbols

τ	time delay
$\hat{\tau}$	time delay estimate
τ_c	the reciprocal of the background noise optical bandwidth ($\Delta\lambda$)
τ_d	pixel dwell time
θ	phase difference between transmitted and received signals
$\hat{\theta}_{ML}$	maximum likelihood phase difference estimate
$U_b(\vec{r}, t)$	complex envelope of the electromagnetic field due to background noise
$U_s(\vec{r}, t)$	complex envelope of the incident field due to a known signal
$y(t)$	output of a post detector filter

Abstract

Line scanning laser sensors which measure range and reflectance are currently being developed to be used as the front end of real-time image processors. This paper establishes the coding combination of intensity modulation and scan pattern for N GaAs laser sources which results in the optimum system performance. A noise model based upon the Poisson point process behavior of a direct (optical intensity) detector is developed. Estimation theory, based upon the Poisson statistics of the detector, is used to develop the maximum-likelihood (ML) processor for both range and reflectance. The realization of the ML estimator for range is shown to be a correlator or matched filter; a suboptimum realization of the reflectance estimator is shown to be a measurement of the detected signal energy, given the range estimate. Performance expressions are presented to relate the variance of the range and the reflectance to the line scan system parameters and the variance of both is shown to be inversely proportional to the detected signal energy. Various combinations of spatial and temporal coding of the N laser sources to separate the return signal energy from each ground resolution cell while increasing the returned energy per cell, are evaluated. Based upon the variance of the range and reflectance estimates, the optimum spatial-temporal coding combinations is chosen. It is shown that if a large maximum unambiguous range is not required, the best performance possible is achieved with N sources scanned in parallel, each source

being sinusoidally modulated. If a large maximum unambiguous range is required, however, the best performance is achieved with N sources scanned in parallel, each source using sinusoidal modulation which is On-Off-Keyed by a pseudo-noise (PN) code.

SPATIAL AND TEMPORAL CODING OF GaAs LASERS FOR A LASER LINE SCAN SENSOR

I. Introduction

The high degree of mobility of modern tactical forces has generated a requirement for near-real-time intelligence. Traditional photographic techniques involve too many delays and too much manual processing. Thus, there is currently a large research and development effort to develop a real-time imagery processing capability. A crude capability would at least provide target cues and coordinate locations to the photo-interpreters. A sophisticated capability would provide threat detection and target recognition information to the pilot of the collection vehicle and radio this same information to behind-the-lines intelligence and plans staffs.

Line scanning laser sensors are currently being developed to be used as the front end of real-time image processors. For some modes of operation range and reflectance data could be obtained from a laser line scan sensor (see block diagram, Fig. 1). Range gating may result in target height profiles (cross-sectional boundaries) which might not be readily apparent from reflectance data alone (due to a low contrast background or camouflage). The target height and reflectance data could be processed by pattern recognition algorithms for target cueing and threat assessment.

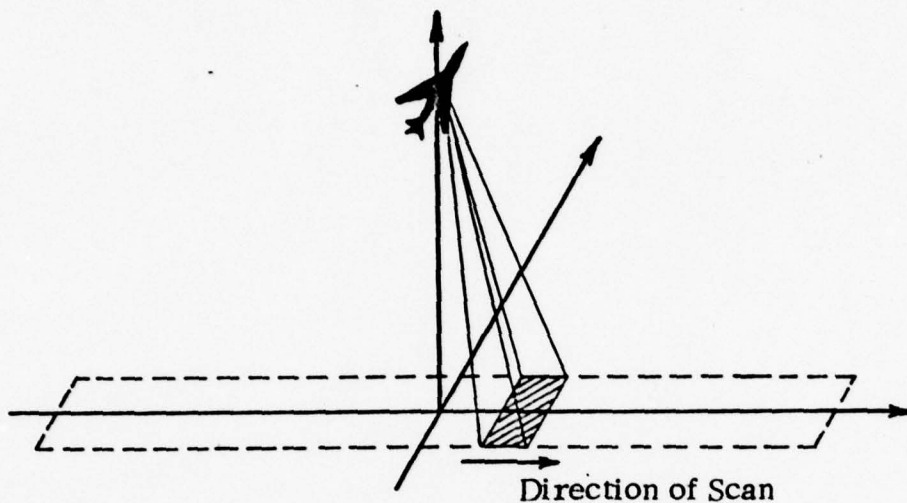


Fig 1. a Basic Laser Line Scanner Geometry

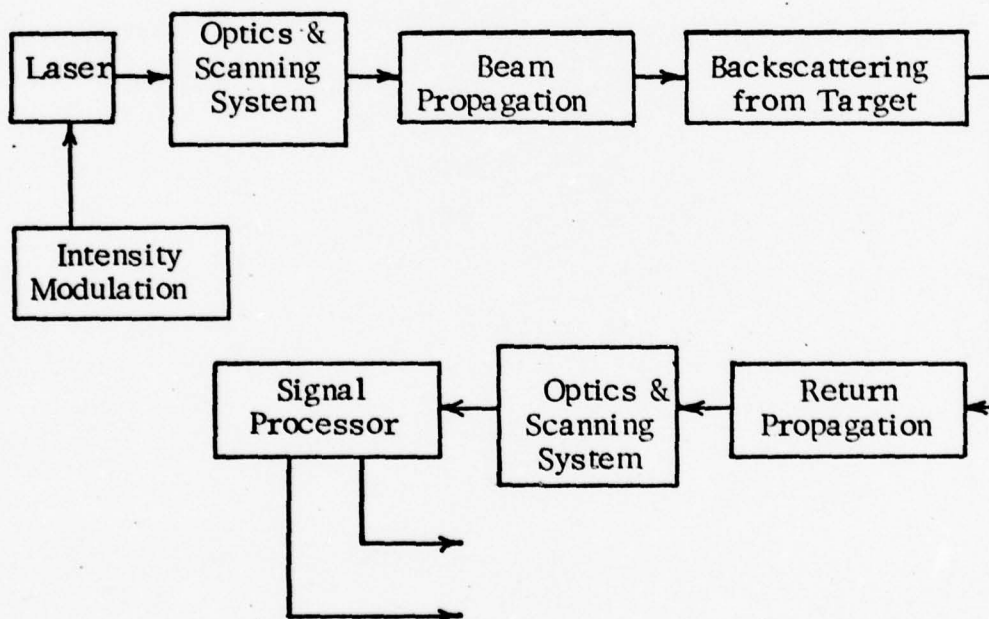


Fig 1. b Block Diagram of a Laser Line Scan Sensor

Fig 1. Basic Geometry and Block Diagram of a Laser Line Scan Sensor

Future operational constraints require small, light, efficient, and rugged laser line scanners. A very favorable source candidate is the semiconductor GaAs laser diode which is very small and light weight. Unfortunately, the GaAs laser is also a low power device, thus requiring the use of many laser diodes to produce the same performance achievable with a larger but more powerful solid state or gas laser. A previous thesis (Ref 1) examined the use of various modulation formats for improved ranging and reflectance estimation using one GaAs laser source. This thesis will investigate various combinations of modulating and scanning techniques for N sources.

Problem

The problem is to obtain the combination of spatial coding (scanning technique) and temporal coding (signal modulation) which will result in an optimum laser terrain mapping system. The purpose of the study is to arrive at, via parameter estimation theory, a mathematical model for a theoretically optimum three-dimensional system, and then try to implement that model with block diagrams based on available technology. The performance of the ideal model will serve as a standard or benchmark to which the performance of real systems may be compared. Problems encountered in implementing the theoretical model will then point to areas requiring further research and development. The goal is for system requirements to drive component technology, rather than research dictating operational systems requirements and performance standards.

Scope and Assumptions

The additive noise model for the photodetector will be limited to signal shot noise, dark current, thermal noise and background noise. The background noise will be assumed to be either additive Gaussian noise (for day time performance estimation) or shot noise associated with a point process (for night time performance estimation). Other noise sources, such as random terrain reflectance, random power fluctuations variations in scan rate, and aircraft vibration will be ignored.

Initially, the sources will be restricted to peak-power-limited (peak power output can never exceed the continuous wave (CW) power output) GaAs laser diodes. The impact of removing the peak-power-limited restriction will be addressed in a later chapter. A recent study indicates that some lasers may not be peak-power-limited (Ref 2: 6-14). GaAs laser diodes have too many lasing modes to be practical in coherent systems, thus, only intensity modulation and direct detection (power) receivers will be considered.

The scanning process will be modeled as if the illuminating laser beam moves discretely from pixel (ground resolution cell) to pixel instead of sliding along the ground in a continuous manner. It will be assumed that the dwell time (illumination time) for each pixel is so short that the inter-pixel smoothing or smearing due to the forward movement of the scanning platform is negligible. The pixel will be assumed to be a square with sides equal to the dimensions of the largest spot formed by

the laser beam projected onto the ground at the extremity of the scan. Also, a square laser beam cross-section will be assumed.

Thesis Overview

The first chapter of this report will cover background theory. The first section will introduce a direct detection statistical model based upon the statistics of the quantum nature of the detection process. The underlying statistics of the detection process will then be used in the following section on parameter estimation and performance theory. Here the maximum likelihood (ML) estimators and Cramer-Rao lower performance bounds (variance) will be developed for both range and reflectance. The root-mean-square (rms) of the Cramer-Rao bounds will be the major tool used in later chapters to compare to performance of various spatial-temporal coding schemes. This chapter will conclude with comments on the implementation of the ML estimators for range and reflectance.

The second chapter will be devoted to the development of potential coding-scanning combinations. It will be followed by a chapter which compares the performance of the various coding-scanning combinations. The report will conclude with a summary/interpretation of the analysis results and recommendations for further research and development.

II. Theoretical Background

The basic tools required to compare the performance of different spatial-temporal coding combinations will be developed in this chapter. The first section will describe the photo-detection process and its statistical additive noise model. The noise statistics introduced in the first section will then be used in the following section on parameter estimation and performance theory. The chapter will conclude with a discussion of implementation of the estimators previously developed.

Direct Detector Statistical Model

The detection of optical energy is accomplished by converting radiant energy into an electrical signal whose amplitude is proportional to the intensity of the incident optical field. Photons (discrete energy packets, or quantum, of light) are absorbed by the photodetector. Some of the absorbed photons excite conduction electrons, thus creating a conduction current $i(t) = q \sum \delta(t-t_i)$, while other absorbed photons cause phonon (or acoustic vibration) heating. The efficiency (percentage of total absorbed photons which excited electrons) is given by the quantum efficiency η . Since the arrival times of photons and the conversion of photons to electrons are both probabilistic in nature, the photodetector current is a random process in time. Therefore the detector output current is a random process regardless of whether the optical field is stochastic or not. In addition, the output current also has components

due to the irradiance from background objects within the detector field-of-view and due to thermal noise processes within the detector, all of which are stochastic processes.

A quantum-mechanically correct description of the direct detection process can be given in terms of the incident optical field and the detector generated current (Ref 3: 1813-1815, 1831-1834). Conditioned on knowing the signal component of the complex envelope of the incident optical field, the detector output is conditionally an inhomogeneous filtered Poisson point process with the rate (intensity) function of

$$\lambda(t) = \underbrace{\beta \int_{A_d} |U_s(\vec{r}, t)|^2 d\vec{r}}_{\lambda_s(t)} + \underbrace{\beta \int_{A_d} E[|U_b(\vec{r}, t)|^2] d\vec{r}}_{\lambda_b(t)} + \lambda_D \quad (1)$$

where

$\lambda(t)$ = rate function (electrons, or events, per second)

β = η/hf_0 = average number of electrons generated per unit of incident optical energy

η = the quantum efficiency of the detector

hf_0 = energy per photon

A_d = detector area

U_s = complex envelope of the incident electromagnetic field due to a known optical signal

U_b = complex envelope of the electromagnetic field due to background noise

$\lambda_s(t)$ = signal rate function

λ_b = average rate function of the optically filtered background noise

E = expected value (ensemble average) operator

λ_D = dark current function

The probability of detecting m photons in the time interval $[0, T]$ is given by

$$P[N(T) = m] = \frac{(\mu)^m}{m!} e^{-\mu}; \quad m = 0, 1, 2, \dots \quad (2)$$

$$\mu = \int_0^T \lambda(\alpha) d\alpha \quad (3)$$

where $N(T)$ is the number of photons detected in the interval. For Eq (1) to be valid, it is required that λ_b be such that $N_b(\tau_c) \ll 1$ where τ_c is the reciprocal of the optical bandwidth of the background noise field. Conditioned on knowing U_s , the joint probability density function of the ordered event times $\{t_i\}$ and the number of events $N(T)$ in an interval $[0, T]$ is given by

$$f_{\{t_i\}, N(T) | U_s} [\{t_i\}, N(T) = m | U_s] = e^{-\int_0^T \lambda(\alpha) d\alpha} \prod_{i=1}^m \lambda(t_i) \quad (4)$$

This is a complete statistical characterization of the detector output.

A partial description is commonly given in the terms of the first and second moments of the filtered detector output current. The filtering may be due to the physical properties of the detector, or may be any external filter between the detector and the signal processor. Let the total detector output current be

$$i_d(t) = q\lambda_s(t) + i_b(t) + i_D(t) + i_{Th}(t) \quad (5)$$

The background noise current may be modeled (Ref 4: 258-259) as a Poisson point process with mean and covariance values of $q\lambda_b$ and $q^2\lambda_b \delta(t-t')$, respectively, so long as $N_b(\tau) \ll 1$. Even in the absence of an incident field upon the detector, there is a current due to thermal generation. This "dark current" may be modeled as a Poisson point process with mean and covariance values of $q\lambda_d$ and $q^2\lambda_d \delta(t-t')$, respectively. The last term in Eq (5), $i_{Th}(t)$, is "thermal noise" due to losses in the detector circuit. It is a Gaussian noise process with zero mean and correlation $2KTR_e^{-1} \delta(t-t')$, where K is Boltzmann's constant, T is the temperature in degrees kelvin, and R_e is the "effective" thermal noise resistance.

The additive noise model for a detector with an output given by Eq (6) is developed in Appendix A and is shown below (Fig 2). The noise process $n(t)$ is zero mean with autocorrelation

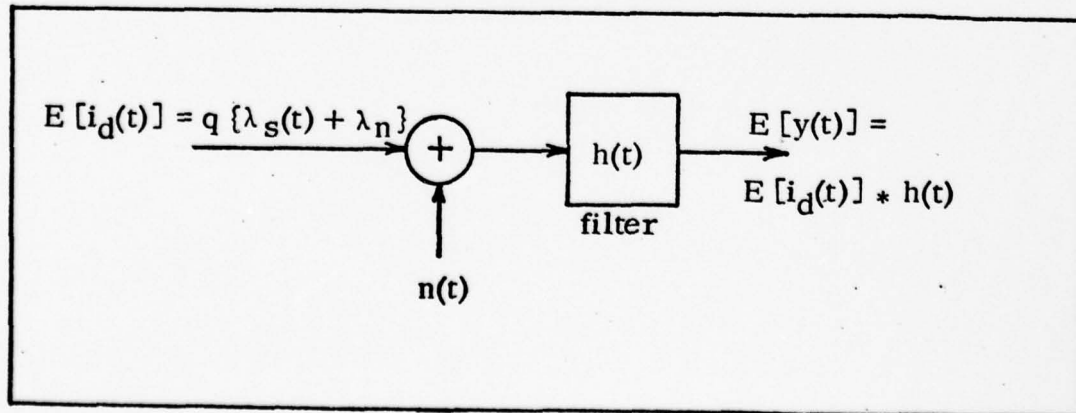


Fig 2. Direct Detector Noise Model

$$R_n(t, t') = [q^2 \lambda_n + 2 \frac{KT}{R_e} + q^2 \lambda_s(t)] \delta(t-t') \quad (6)$$

where $\lambda_n = \lambda_b + \lambda_d$. The terms $q^2[\lambda_n + \lambda_s(t)]$ are the autocorrelation of what is commonly known as "shot noise".

Thus $n(t)$ is a white, zero mean, non-stationary, and non-Gaussian noise process. This means (strictly speaking) that frequency domain techniques, i.e., Fourier Transform techniques, which require stationary, cannot be used to calculate signal-to-noise ratio (SNR) and other useful performance parameters. It also means that all of the classical radar results, such as using SNR to calculate probability of error, are not applicable because they are based upon Gaussian statistics.

There are two cases when frequency domain techniques may be used. The first case requires the DC component of $\lambda_s(t)$, denoted λ_o , to be much larger than the time varying fluctuations of $\lambda_s(t)$. Then Eq (6) becomes

$$R_n(\tau) = [q^2(\lambda_n + \lambda_o) + 2 \frac{KT}{R_e}] \delta(\tau) \quad (7)$$

where $\tau = t-t'$. Now $n(t)$ is a white, approximately stationary Poisson noise process with noise power spectral density

$$S_n(f) = q^2(\lambda_n + \lambda_o) + 2 \frac{KT}{R_e} \quad (8)$$

This is commonly referred to as the "signal shot noise limited case". The second case occurs when $q^2 \lambda_n$ is the dominant term in Eq (6). This is very often the case for real world detectors when the background noise intensity is large and cooled detectors ($i_{Th} \approx 0$) are used. Eqs (7) and (8) then become

$$R_n(\tau) = q^2 \lambda_n \delta(\tau) \quad (9)$$

$$S_n(f) = q^2 \lambda_n \quad (10)$$

This is usually referred to as the "background noise limited case".

If the rate function becomes very large, then the filtered Poisson process may be modeled as a Gaussian process. In general when

$$\frac{\lambda_n + \lambda_0}{\text{Bandwidth of } h(t)} \gg 1 \quad (11)$$

the filter output looks like a Gaussian random process with mean $\bar{n} = q\lambda(t)$ and variance $\sigma_n^2 = \lambda(t) \int_{-\infty}^{\infty} h^2(t) dt$ (Ref 5: 127-131). Thus, although $n(t)$ is not Gaussian, since a filtered Gaussian random process is also Gaussian, $n(t)$ may be modeled as being Gaussian by looking backward into the filter from the output. For this specific case, given by Eq (11), $n(t)$ is a white, approximately stationary, and approximately Gaussian noise process with autocorrelation and power spectral density given by Eqs (7) and (8), respectively.

In summary, the output current of the photodetector is a conditional Poisson point process with a second moment additive noise model as shown in Fig 1. The autocorrelation of the additive noise is (in general) impulsive and non-stationary. Only in the less interesting cases of "signal shot noise limited", or when the noise rate function is much greater than the bandwidth of $h(t)$, can the noise be modeled as Gaussian and traditional radar results be used to analyze the optical system. In the more practical case of "background noise limited" new performance techniques must be developed using Poisson statistics.

Parameter Estimation and Performance Theory

This section will have three parts. The first will develop the maximum likelihood (ML) estimators for both range and reflectance using Poisson statistics. It will also discuss the structure imposed upon the signal processor by the ML estimators. The second part will use Poisson statistics to derive the Cramer-Rao (CR) performance lower bounds in general, and will look at the CR bounds for several specific modulation techniques. The third part will compare the CR bounds developed using Poisson statistics with those developed previously using Gaussian statistics (Ref 1: 21-56).

Maximum Likelihood Parameter Estimation. The principle behind the measurement of range and reflectance by the laser line scan system is very similar to that of a classical radar. As with a radar, the time delay (or phase difference) between a transmitted signal and its return is proportional to the target range. In addition, the return signal amplitude will be proportional to the target reflectance.

All measurements of the actual values of the delay τ and the reflectance ρ will be degraded by system noise, and thus will only be estimates of the true values. These estimates, denoted $\hat{\tau}$ and $\hat{\rho}$, are based upon the observation of the ordered event times $\{t_i\}$ of detected electrons and the number of events $N(T)$ in an interval $[0, T]$. The desire is to use statistical tools available to determine a signal processor such that $E[\hat{\tau}] = \tau$ (zero bias) and $\text{var} [\tau - \hat{\tau}]$ (a measure of how close the estimate $\hat{\tau}$

is to the real value τ) is small (with similar expressions for $\hat{\rho}$ and ρ). Since no a priori information about the random parameters τ and ρ is known, maximum likelihood (ML) estimation will be used. Given the observation A , the ML estimate of the random parameter A is defined by the likelihood function

$$\begin{array}{l} \text{Maximize} \\ \text{by Choice} \\ \text{of } A \end{array} \left\{ f_{Z|A}(Z|A) \right\} \Big|_{A = \hat{a}_{ML}(Z)} \quad (12)$$

Ref 6: 63), or equivalently, the log likelihood function

$$\begin{array}{l} \text{Maximize} \\ \text{by Choice} \\ \text{of } A \end{array} \left\{ \ln f_{Z|A}(Z|A) \right\} \Big|_{A = \hat{a}_{ML}(Z)} \quad (13)$$

where $f_{Z|A}(Z|A)$ is the conditional probability density function of (pdf) of the observation Z , conditioned on knowing the parameter A . For convenience, the subscripts will be dropped from the traditional notation for pdf's and N_T will be used to represent $N(T) = m$. From Eq (13) it follows that a sufficient, though not necessary, condition for ML estimate can be found from the log likelihood equation $l(A)$ given by

$$l(A) \triangleq \frac{\partial \ln[f(Z|A)]}{\partial A} \Big|_{A = \hat{a}_{ML}(Z)} = 0 \quad (14)$$

From Eq (4), the conditional joint probability density function for the direct detector observations is given by

$$f(\{t_i\}, N_T | \tau, \rho) = \exp \left[- \int_0^T \lambda(\alpha) d\alpha \right] \prod_{i=1}^m \lambda(t_i) \quad (15)$$

The rate function in Eq (14) is given by rewriting Eq (1) as

$$\lambda(t) = \lambda_s(t) + \lambda_n \quad (16)$$

$$\lambda_s(t) = \rho s t = \rho \beta P_d m(t) ; \quad |m(t)| \leq 1 \quad (17)$$

where $m(t)$ is the intensity modulation impressed upon the transmitter, and the detector power P_d is the peak power limited (CW) laser output P_t times all other gain and loss mechanisms such as atmospheric absorption, transmitter and receiver field-of-view, and receiver aperture area. Substituting Eqs (15) and (16) into Eq (13) yields

$$\begin{aligned} \ell_n[f\{t_i\}, N_T | \tau, \rho] &= \sum_{i=1}^m \ell_n[\rho s(t_i - \tau) + \lambda_n] \\ &\quad - \int_0^T [\rho s(\alpha - \tau) + \lambda_n] d\alpha \end{aligned} \quad (18)$$

The simultaneous estimators $\hat{\tau}$ and $\hat{\rho}$ may be found by substituting Eq (18) into the simultaneous equations

$$\left. \frac{\partial \ell_n[f\{t_i\}, N_T | \tau, \rho]}{\partial \tau} \right|_{\tau = \hat{\tau}} = 0 \quad (19)$$

$$\left. \frac{\partial \ell_n[f\{t_i\}, N_T | \tau, \rho]}{\partial \rho} \right|_{\rho = \hat{\rho}} = 0 \quad (20)$$

and solving simultaneously for $\hat{\tau}$ and $\hat{\rho}$. Using

$$\frac{\partial}{\partial \tau} s(t - \tau) = -\frac{d}{dt} s(t - \tau) = -s(t - \tau) \quad (21)$$

substituting Eq (18) into Eq (19), rearranging and canceling like terms gives

$$\sum_{i=1}^m \frac{\dot{s}(t-\tau)}{\rho s(t-\tau) + \lambda_n} \bigg|_{\substack{t=t_i \\ \tau=\hat{\tau}}} = \int_0^T \frac{\partial}{\partial \alpha} s(\alpha-\tau) d\alpha \quad (22)$$

The righthand side of Eq (22) becomes $s(T-\tau) - s(-\tau) = 0$ for periodic modulation signals, or if the observation interval $[0, T]$ is much greater than delay τ so that "end effects" may be ignored,

$$\sum_{i=1}^m \frac{\dot{s}(t-\tau)}{\rho s(t-\tau) + \lambda_n} \bigg|_{\substack{t=t_i \\ \tau=\hat{\tau}}} = 0 \quad (23)$$

Substituting Eq (18) into Eq (20) and rearranging terms gives

$$\sum_{i=1}^m \frac{s(t-\tau)}{\rho s(t-\tau) + \lambda_n} \bigg|_{\substack{t=t_i \\ \rho=\hat{\rho}}} = \int_0^T s(\alpha-\tau) \partial \alpha = Q, \text{ a constant} \quad (24)$$

The simultaneous solution of Eqs (23) and (24) for $\hat{\tau}$ and $\hat{\rho}$ would give the joint estimates for delay and reflectance respectively. Unfortunately, Eqs (23) and (24) are inseparable and there is no solution for $\hat{\tau}$ independent of $\hat{\rho}$ and vice-versa.

However, the form of Eq (18) is that of a correlator. This may be seen by recalling that $i(t) = q \sum_{i=1}^m \delta(t-t_i)$. If $i(t)$ is multiplied by $q^{-1} \ln \lambda(t)$ and integrated using the sifting property of the impulse function, the result is

$$\int_0^T q \sum_{i=1}^m \delta(t-t_i) q^{-1} \ln \lambda(t) dt = \sum_{i=1}^m \ln \lambda(t_i) \quad (25)$$

Now subtracting a constant $Q = \int_0^T \lambda(\alpha) d\alpha$ and substituting Eq (16), the result is Eq (18)

$$\ln[f(\{t_i\}, N_T | \tau, \rho)] = \sum_{i=1}^m \ln[\rho s(t_i - \tau) + \lambda_n] - \int_0^T [\rho s(\alpha - \tau) + \lambda_n] d\alpha \quad (18)$$

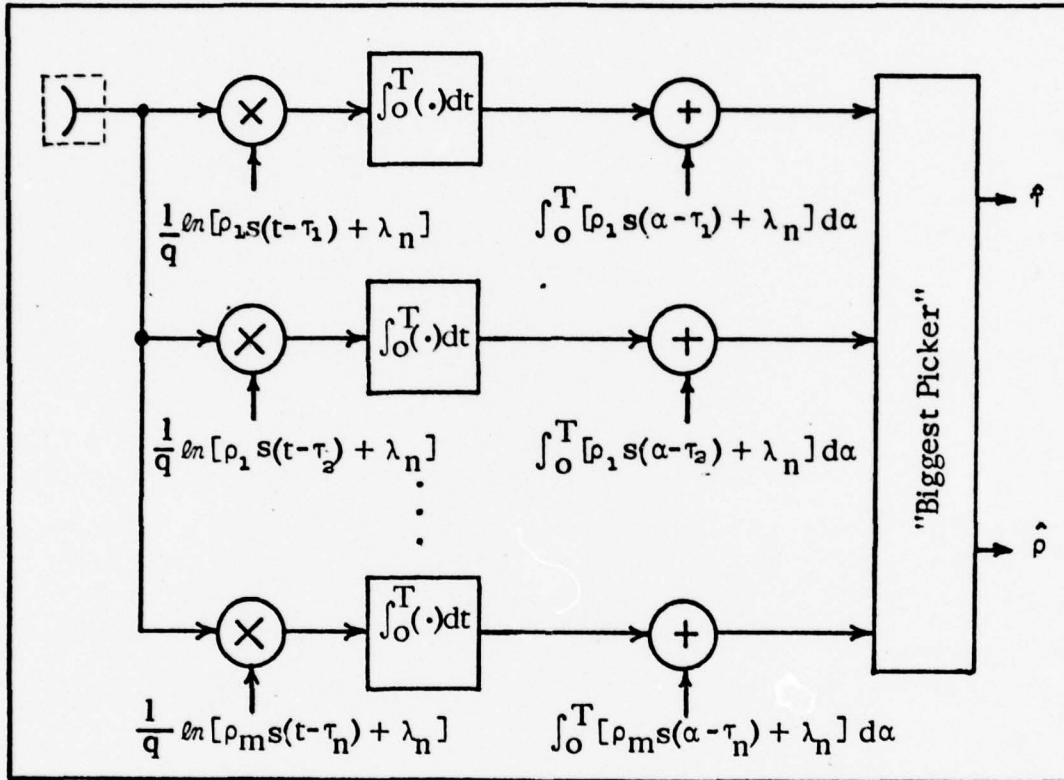


Fig. 3 $m \times n$ Bank of Correlators Implementation of ML Estimators

which may be realized approximately by the $m \times n$ bank correlations shown above (Fig 3). The "biggest picker" picks the output of the correlator with the largest amplitude and the ρ_i and τ_j that corresponds to that correlator are the estimates $\hat{\rho}$ and $\hat{\tau}$, respectively. The correlator realization shown above requires $m \times n$ correlators and is not practical to implement.

The correlator input $q^{-1} \ln [\rho s(t) + \lambda_n]$ may be written as

$$\frac{1}{q} \ln \left[\lambda_n \left(1 + \rho \frac{s(t)}{\lambda_n} \right) \right] = \frac{\ln \lambda_n}{q} + \frac{1}{q} \ln \left[1 + \rho \frac{s(t)}{\lambda_n} \right] \quad (26)$$

If $\lambda_n \gg \rho s(t)$, then the second term on the righthand side of Eq (26) may be expanded using a series expansion. Keeping only the first term of the expansion, Eq (26) equals

$$\frac{1}{q} \ln \lambda_n + \frac{1}{q} \rho \frac{s(t)}{\lambda_n} \quad (27)$$

The likelihood equation, given by Eq (18), may now be rewritten as

$$\text{Maximize}_{\rho, \tau} \left[\int_0^T i(t) \frac{1}{q} \rho \frac{s(t)}{\lambda_n} dt - \int_0^T (\rho s(\alpha - \tau) + \lambda_n) d\alpha \right] \quad (28)$$

Keeping only the ρ and τ dependent terms, Eq (26) becomes

$$\text{Maximize}_{\rho, \tau} \left[\int_0^T \frac{i(t)}{q} \rho \frac{s(t)}{\lambda_n} dt - \int_0^T \rho s(\alpha - \tau) d\alpha \right] \quad (29)$$

The first term in Eq (29) describes the correlator. Now the detector current $i(t)$ is correlated with a linear function of $s(t)$, as in familiar radar applications. If the observation interval $[0, T]$ is much greater than the largest expected delay τ , i. e., if end effects can be ignored, then the last term in the brackets can be ignored.

A practical (suboptimum) estimator realization is shown below (Fig 4).

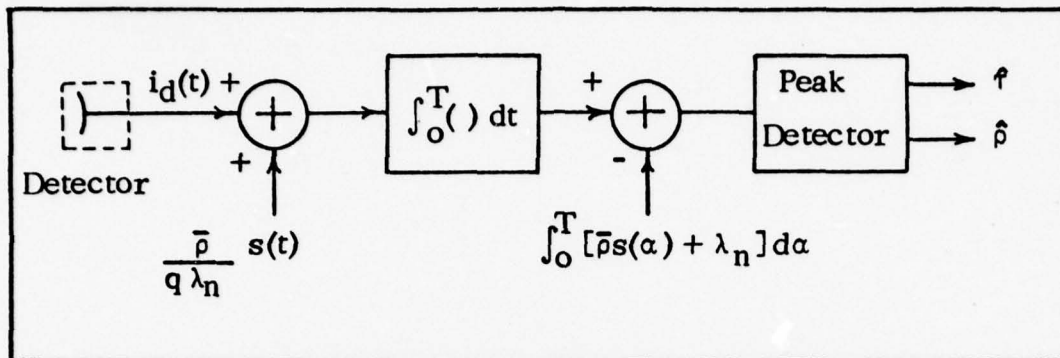


Fig 4. Suboptimum ML Estimators

The delay between the transmission of the signal and the occurrence of a peak is equal to $\hat{\tau}$. The amplitude of the peak detector output, given the delay estimate $\hat{\tau}$, is proportional to the reflectance estimate $\hat{\rho}$.

Note that, in general, the detector output is not correlated with $s(t)$, as would be done in a conventional radar, but instead is correlated with the weighted natural log of $\rho s(t) + \lambda_n$. Thus, once again, it must be stressed that classical radar techniques do not always apply to optical systems involving direct (power) detection. Only in the background noise limited case may the familiar radar ML estimator be used optimally.

Cramer-Rao Lower Performance Bounds. It was stated in the previous section that it is desirable that $\text{var} [\tau - \hat{\tau}]$ and $\text{var} [\rho - \hat{\rho}]$ be small. These variances are very difficult to compute; therefore, a lower bound for the variances will be computed using the Cramer-Rao (CR) lower bound. The CR lower bound for the variances of the estimator errors for τ and ρ is defined as

$$\sigma_j^2 \triangleq \text{var} [\hat{a}_j(\{t_i\}, N_T) - A_j] \geq J_{jj} \quad (30)$$

where J_{jj} is the jj th element of the 2×2 square matrix \underline{J}^{-1} (Ref 6: 79).

The elements of \underline{J} are

$$J_{jk} = -E \left[\frac{\partial^2 \ln f(\{t_i\}, N_T | \tau, \rho)}{\partial A_j \partial A_k} \right] \quad (31)$$

where $A_1 = \tau$ and $A_2 = \rho$. The CR lower bound is an optimistic performance measure. It indicates that, regardless of how good the signal processor, the smallest error variance possible occurs when Eq (30) achieves equality. Such a processor is called an efficient estimator. Any sub-optimum process will result in an error variance larger than the lowest limit given by Eq (30).

The elements of \underline{J} may be evaluated by substituting Eq (18) into Eq (31), using Eq (21) and the observation that

$$E \left[\sum_{i=1}^m \rho s(t_i - \tau) \right] = E \left[\int_0^T \frac{i(t)}{q} \rho s(t - \tau) dt \right] = \int_0^T \frac{\overline{i(t)}}{q} \rho s(t - \tau) dt \quad (32)$$

where $i(t) = q \sum_{i=1}^m \delta(t - t_i)$ and $E[i(t)] = (\rho s(t - \tau) + \lambda_n)q = \overline{i(t)}$. The elements of \underline{J} are then

$$J_{\tau\tau} = \int_0^T \frac{\rho^2 \dot{s}^2(t - \tau)}{\rho s(t - \tau) + \lambda_n} dt \quad (33)$$

$$J_R = \int_0^T \frac{\dot{s}(t - \tau)s(t - \tau)}{\rho s(t - \tau) + \lambda_n} dt \quad (34)$$

$$J_{\rho\rho} = \int_0^T \frac{s^2(t - \tau)}{\rho s(t - \tau) + \lambda_n} dt \quad (35)$$

It can be shown that, in the limiting cases of $\lambda_n \gg \rho s(t-\tau)$ or $\lambda_n \ll \rho s(t-\tau)$ Eq (34) is equal to zero so long as $s(t)$ is periodic or the observation interval $T \gg \tau$. Therefore, substituting Eqs (33) and (35) into Eq (30) gives

$$\sigma_\tau^2 \geq \left[\int_0^T \frac{\rho^2 \dot{s}^2(t-\tau)}{\rho s(t-\tau) + \lambda_n} dt \right]^{-1} \quad (36)$$

$$\sigma_\rho^2 \geq \left[\int_0^T \frac{s^2(t-\tau)}{\rho s(t-\tau) + \lambda_n} dt \right]^{-1} \quad (37)$$

It can be shown that these two equations become (i) for $\lambda \gg \rho s(t)$

(Background Noise Limited Case):

$$\sigma_\tau^2 \geq \frac{\lambda_n}{\rho^2 E_{S_{BPF}}^2 B_S^2} \quad (38)$$

$$\sigma_\rho^2 \geq \frac{\lambda_n}{E_S} \quad (39)$$

(ii) for $\lambda_n \ll \rho s(t)$ (Signal Shot Noise Limited Case):

$$\sigma_\tau^2 \geq \frac{k}{\rho^2 E_{S_{BPF}}^2 B_S^2} \quad (40)$$

$$\sigma_\tau^2 \geq \frac{\rho}{\int_0^T s(t) dt} \quad (41)$$

(Ref 5: 308-309), where

$$B_S^2 \triangleq \frac{\int_{-\infty}^{\infty} \omega^2 S(\omega) d\omega}{\int_{-\infty}^{\infty} S(\omega) d\omega} = 4\pi^2 \frac{\int_{-\infty}^{\infty} f^2 |F_S(f)|^2 df}{\int_{-\infty}^{\infty} |F_S(f)|^2 df} \quad (42)$$

$$E_S \triangleq \int_0^T S^2(t) dt = \int_{-\infty}^{\infty} |F_S(f)|^2 df \quad (43)$$

and $F_s(f)$ is the Fourier Transform of $s(t)$. The subscript BPF denotes "bandpass filtered", k is a constant of proportionality, arbitrarily set equal to one, and has units of seconds⁻¹. The parameter B_s is the normalized effective (or rms) bandwidth of $s(t)$ where $s(t)$ is defined by Eq (17). The parameter E_s is proportional to the energy of the envelope of the intensity of the incident optical field. One may also think of E_s as the energy of $i_s(t) = q\lambda_s(t)$, i.e., the post detector signal energy. Also note that $\int_0^T s(t)dt$ is just the average number of photons detected over an observation interval $[0, T]$ and is proportional to the energy of the complex envelope of the incident optical field. Thus, in both limiting cases, the mean square error of both \hat{f} and $\hat{\beta}$ may be reduced by increasing E_s , and consequently $\int_0^T s(t)dt$. Also, the mean square error of $\hat{\tau}$ depends upon the mean square bandwidth of $s(t)$. The mean square error of \hat{f} will be minimized by making the mean square bandwidth as large as possible.

There is another interpretation of Eqs (36) and (37) for the signal shot noise limited case which will be presented for the sake of completeness (Ref 7: 85-86). If the intensity modulated signal $s(t)$ is represented in terms of the complex field $U_s(r, t)$, then

$$\lambda_s(t) = \rho\beta A_d |U_s(\vec{r}, t)|^2 \quad (44)$$

For $\lambda_n \ll s(t)$, Eqs (35) and (36) become

$$\sigma_\tau \geq \frac{1}{4\rho\beta A_d E |U|^2 |U|} \quad (45)$$

$$\sigma_p^2 \geq \frac{\rho}{\beta A_d E |U|} \quad (46)$$

$E |U|$ and $B^2 |U|$ are the energy and the mean square bandwidth of the incident optical field, respectively.

In the following section (Additional Comments on Implementation) it will be shown that the mean square bandwidth and energy of all pulse code modulation schemes to be considered in this report are approximately

$$B_{PC}^2 \approx 8 t_0^{-2} ; \rho \gg 1 \quad (47)$$

$$E_s = \frac{\beta^2 P_d^2 \tau_d}{4} = \frac{\beta^2 P_d^2 \rho t_0}{4} \quad (48)$$

where t_0 is the pulse duration $\tau_d = \rho t_0$ is the dwell time and code word length, and ρ is the number of chips in the pulse code sequence or word. Since the slant range to a pixel is given by $r = c\tau/2$ where c is the speed of light and τ is the round trip time delay, it can be shown that the range error variance is related to the time error variance by

$$\sigma_r^2 = \frac{c^2}{4} \sigma_\tau^2 \quad (49)$$

Substituting Eqs (47) - (49) into Eqs (38) - (41) gives the CR lower performance bound for pulse code modulation:

$$\text{Background Noise Limited} \left\{ \begin{array}{l} \sigma_{r\text{-PEM}}^2 \geq \frac{c^2 \lambda_n t_o^2}{8 \rho^2 \beta^2 P_d^2 \tau_d} = \frac{c^2 \lambda_n t_o}{8 \rho^2 \beta^2 P_d^2 p} \end{array} \right. \quad (50)$$

$$\left\{ \begin{array}{l} \sigma_{p\text{-PEM}}^2 \geq \frac{2 \lambda_n}{\beta^2 P_d^2 \tau_d} = \frac{2 \lambda_n}{\beta^2 P_d^2 p t_o} \end{array} \right. \quad (51)$$

$$\text{Signal Shot Noise Limited} \left\{ \begin{array}{l} \sigma_{r\text{-PEM}}^2 \geq \frac{c^2 t_o^2}{8 \rho^2 \beta^2 P_d^2 \tau_d} \end{array} \right. \quad (52)$$

$$\left\{ \begin{array}{l} \sigma_{p\text{-PEM}}^2 \geq \frac{2 \rho}{\beta P_d \tau_d} \end{array} \right. \quad (53)$$

Mean square bandwidth has little meaning for sinusoidal (harmonic) modulation. Therefore, the CR bounds must be evaluated by letting $s(t)$ be given by

$$s(t) = \beta \frac{P_d}{2} [1 + \sin 2\pi f_m t] \quad (54)$$

and substituting directly into Eqs (36) - (37). After some calculus and using Eq (49), the CR lower performance bounds for sinusoidal modulation are:

$$\text{Background Noise Limited} \left\{ \begin{array}{l} \sigma_{r\text{-s}}^2 \geq \frac{c^2 \lambda_n}{2 \pi^2 f_m^2 \rho^2 \beta^2 P_d^2 \tau_d} \end{array} \right. \quad (55)$$

$$\left\{ \begin{array}{l} \sigma_{p\text{-s}}^2 \geq \frac{8 \lambda_n}{3 \beta^2 P_d^2 \tau_d} \end{array} \right. \quad (56)$$

$$\text{Signal Shot Noise Limited} \left\{ \begin{array}{l} \sigma_{r\text{-s}}^2 \geq \frac{c^2}{8 \pi^2 f_m^2 \rho \beta P_d \tau_d} \end{array} \right. \quad (57)$$

$$\left\{ \begin{array}{l} \sigma_{p\text{-s}}^2 \geq \frac{2 \rho}{\beta P_d \tau_d} \end{array} \right. \quad (58)$$

The CR bounds expressed by Eqs (50) - (53) and Eqs (55) - (58) will be used extensively in Chapter III comparing the various spatial-temporal coding combinations.

At this point it should be noted that if the peak power limited restriction is removed, and if P_t increases by the same factor for both PCM and sinusoidal modulation, then E_s will increase the same way for both modulation types. Furthermore, if the rms power transmitted is allowed to be a constant regardless of the modulation used, then E_s will be identical for both modulation types. Eqs (35) - (37) indicate that if E_s is always the same, then the reflectance performance will be independent of the type modulation used, and the range performance will depend only upon the mean square bandwidth of the modulation scheme.

CR Bounds: Gaussian Versus Poisson Statistics. One might ask how the Poisson performance bounds compare with those developed by Chapuran using Gaussian statistics (Ref 1: 25-26, 54). In order to make a comparison, the Gaussian noise power spectral density is defined to be

$$\frac{N_0}{2} = \begin{cases} \lambda_0 & ; \text{Signal Shot Noise Limited Case} & (59) \\ \lambda_n & ; \text{Background Noise Limited Case} & (60) \end{cases}$$

where λ_0 is the direct current (DC) component of $\lambda_s(t)$ as defined by Eq (17). It must be noted that the definition of the mean square bandwidth for pulse code modulation used by Chapuran is 2π larger than that used in this paper and that reflectance is hidden in Chapuran's definition

of detected power. After making the proper definition adjustments, a direct comparison of the Gaussian and Poisson results for both pulse code modulation and sinusoidal modulation reveals that in every case but one the rms error is larger for the Gaussian case. The one exception occurs for the rms error of range estimation for the background noise limited case using pulse code modulation. For this specific case the rms errors were the same for both the Gaussian and the Poisson results. Thus, "quick and dirty" performance "questimates" may be made using the appropriate $N_0/2$ for the Gaussian statistical CR bounds so long as it is realized the performance results will be pessimistic. However, for a more exact and careful performance analysis, the CR performance bounds developed using Poisson statistics must be used whenever a direct detection optical detector is used in the background noise limited regime.

Additional Comments on Implementation

This section will discuss the implementation of ML estimators for τ and ρ utilizing matched filters. Matched filters and their performance characteristics (in general), one-shot matched filters, and closed loop estimators will be discussed in turn. The section will conclude with a few brief comments on transmitter and receiver optics, background noise, and typical limiting cases for operational deployment.

Matched Filters in General . The ML estimator for a direct detector (developed earlier in this chapter) is a correlator. It can be shown that correlators and matched filters are equivalent methods for synthesizing the same ML estimator (Ref 8: 315-317). If the output of a receiver $y(t) = m(t) + n(t)$ is passed through a matched filter with impulse response $h(t) = s(t_0 - t)$, the output of the filter is just the time autocorrelation of the signal, and is given by

$$R(\tau) = \int_{t_0}^{T+t_0} s(\alpha) s(\alpha + \tau) d\alpha \quad (61)$$

The output of the matched filter peaks when $\tau = t_0$ and its amplitude is proportional to the received signal energy. Thus, the output of a direct detector may be processed via a matched filter. The output may be routed to a peak detector. The elapsed time between the transmission of the signal and the occurrence of a peak is the delay estimate, and the amplitude of the peak is proportional to the reflectance estimate.

The matched filter realization of the ML estimator is shown below (Fig 5). Note that the filter impulse response is the time inverse of the correlator reference input. Therefore, the restriction that applied to using established radar techniques for optical detection using correlators also hold for optical detection using matched filters.

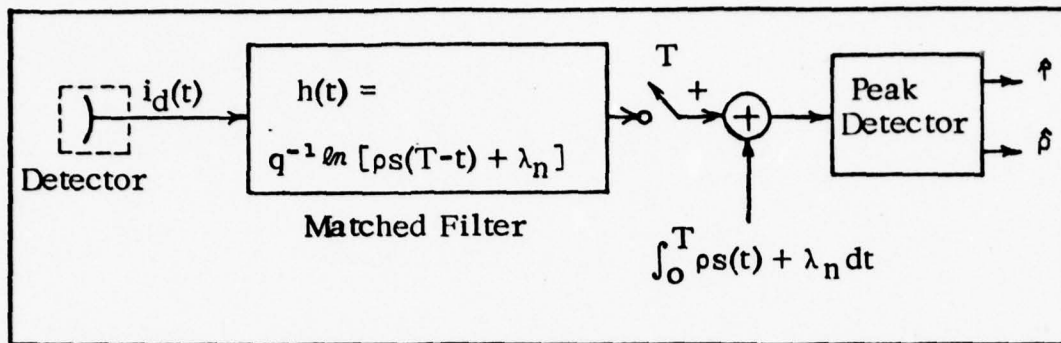


Fig 5. Matched Filter Implementation of ML Estimators

In order to make the signal $s(t)$ and its autocorrelation straight forward, several simplifying assumptions will be made. It will be assumed that both range and reflectance are constant in a pixel. Also, it will be assumed that there is no significant spatial filtering caused by scanning a beam over the ground. Recall that the scanning process is to be modeled as if the illuminating beam moves discretely from pixel to pixel.

The idealized autocorrelation of a pulse is a triangular shaped lobe (Fig 6). The CR lower bound assumes that the matched filter output is a single lobe, and it computes the error bound of noise perturbations about this lobe. If the matched filter output (autocorrelation) has large

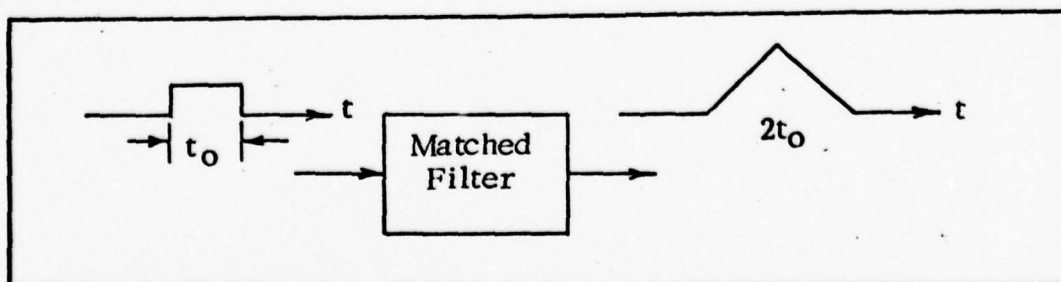


Fig 6. Matched Filter Response for a Single Pulse

sidelobes, then a noise spike added to a sidelobe could be larger than the peak of the mainlobe, thus causing an additional error in the delay measurement (Fig 7). This is the problem of global accuracy versus local accuracy which is discussed in the literature (Ref 9: 294-307). Therefore,

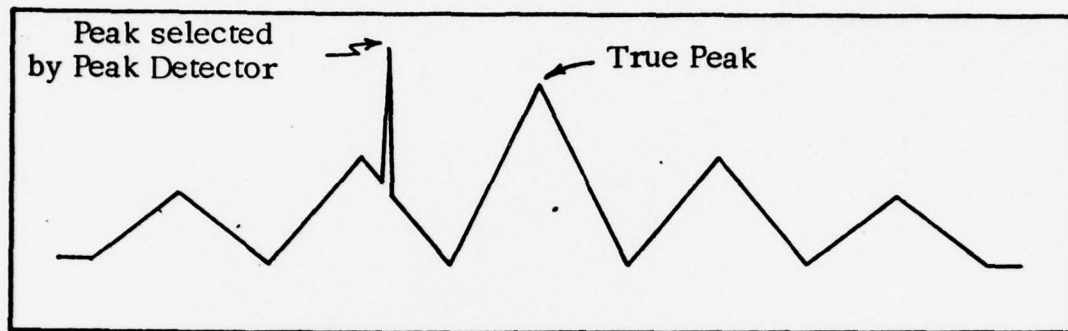


Fig 7. Error Due to Large Sidelobes Plus a Noise Spike

it is desirable to use pulse codes for $s(t)$ that have bi-level autocorrelations, i.e., whose autocorrelation peaks when $\tau = 0$, and is a constant for $\tau \neq 0$ (Fig 6). Pseudo-noise (PN) codes, Barker codes, Totally Orthogonal Complementary Pair codes, and others have bi-level autocorrelations.

As stated earlier, the range is derived from the delay estimate through the expression $r = c\tau/2$. However, since the transmitted signal is periodic with period T , a signal return for $s(\tau)$ looks just like a return for $s(\tau + nT)$ where n is an integer. This implies

$$r = \frac{c(\tau \text{ modulo } T)}{2} \quad (62)$$

Thus, the maximum unambiguous range that may be measured is given by

$$R_{\text{amb}} = \frac{cT}{2} \quad (63)$$

where T is the dwell time. From Eqs (50) and (52), the range performance will be best when $T = \tau_0 = p t_0$, where t_0 is as small as permitted by the limiting bandwidth of the transmitter or detector, whichever is smallest.

Range resolution is a measure of how small the slant range between two objects may be and still be distinguished from one another by the range estimator. Since each pixel is assumed to have a constant range, range resolution is of no significance to this system and will not be evaluated for each different modulation scheme.

One-Shot Matched Filters. The autocorrelation of a signal as defined by Eq (61) may be accomplished by "sliding" the signal past a replica of itself while at the same time multiplying and integrating. This is usually accomplished by "sliding" the signal through a matched filter, normally a delay line summer. Since the performance is best when a code word is τ_d long (as shown later), a code word reflected by a given pixel gets to "slide" through the matched filter only once; hence, the name "one-shot" matched filter. This is the type of matched filter that will be used to process the pulse code modulation schemes considered in this report.

PN codes are well known and are easy to generate using shift registers (Ref 10: 143-152). The normalized autocorrelation of a PN code p chips long is bi-level, periodic (or circular), and has minimum correlation of $-1/p$ (Fig 8). However, in order for the autocorrelation to be bi-level with no sidelobes, many PN codewords must slide through a matched filter which is matched to several codewords. If two adjacent pixels are more than ct_0 distance apart the string of continuous codewords will be broken and sidelobes will appear in the matched filter output. Thus, the chip duration t_0 should be longer than the maximum $\Delta\tau$ expected between adjacent pixels. Unfortunately, as shown by Eq (50), this degrades the range estimation performance. Another approach might be to transmit at least three code words per pixel. This would require that $p'=p/3$, and again Eq (50) indicates that the performance will be degraded. The choice of which of the two approaches is best depends upon the maximum $\Delta\tau$ expected and the minimum t_0 the system is capable of achieving. It should be pointed out there are other classes of periodic pulse codes that, although they do not have a bi-level autocorrelation function, have relatively small sidelobe structures and may be used for ranging. Many times these codes are found via exhaustive computer searches, and thus are not considered here.

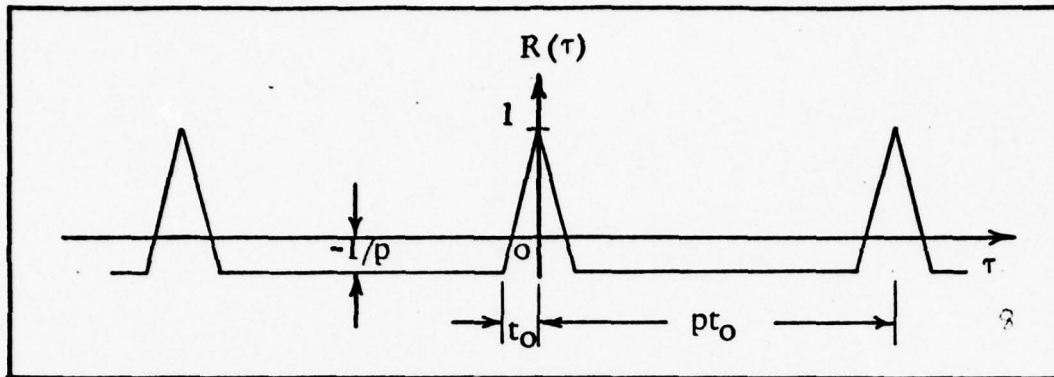


Fig 8. Normalized Autocorrelation of PN Code p Chips Long

The approximate mean square bandwidth of a PN code was calculated by Chapuran (Ref 1: 83-87) using the definition for B_s^2 given by Eq (42). The power spectral density $S(\omega)$ for a PN code has a $(\sin x/x)^2$ distribution, and, strictly speaking, has infinite bandwidth. Chapuran assumed that the significant portion of the spectrum envelope only extended out to the second zero crossing on each side of the double sided spectrum. Thus, the resulting mean square bandwidth is only approximate. However, it is good for most realizable systems since real systems do not generate pulses with zero rise and fall times. Thus the results are approximate for a wide variety of pulse formats, not just for square pulses. Unfortunately, it can be shown that the definition which he used for the power spectral density for a PN code $S_{PN}(\omega)$ was 2π times too small. Making the proper adjustment, the mean square bandwidth for a PN code is given by

$$B_{PN}^2 = \frac{8(p+1)}{pt_0^2} \approx \frac{8}{t_0^2} ; p \gg 1 \quad (64)$$

The output power of the laser can be represented by

$$P(t) = \frac{P_t}{2} \left[1 + \sum_{i=0}^{p-1} a_i \{ U[t - it_0] - U[t - (t+1)t_0] \} \right]; 0 \leq t \leq \tau_d \quad (65)$$

where $A = \pm 1$, and $U(t)$ is the unit step function. Therefore the bandpass filtered detector current signal energy given by Eq (41) is found to be

$$E_{PN-BPF} = \frac{\beta^2 P_d^2 \tau_d}{4} = \frac{\beta^2 P_d^2 p t_0}{4} \quad (66)$$

due to the DC component, where $E_{PN} = 2 E_{PN-BPF}$ (67)

Totally Orthogonal Complimentary Code pairs are two sets of complimentary pairs A and B such that

$$R_A(\tau) + R_B(\tau) = \begin{cases} 2p \left(1 - \frac{|\tau|}{t_0} \right); & |\tau| \leq t_0 \\ 0; & \text{elsewhere} \end{cases} \quad (68)$$

Where p is the number of chips in A or B, and t_0 is the chip duration (Ref 11: 2-16) (Fig 9). CP codes are also aperiodic, i.e., the code has to slide past a replica of itself only once to generate an autocorrelation peak with no sidelobes. Therefore, CP codes do not exhibit the problem encountered with PN codes which required $\Delta\tau < t_0$. Thus, CP codes may be used to distinguish sharp range boundaries without any loss of performance.

CP codes require that both code word "A" and its compliment "B", illuminate each pixel. Unfortunately, the sum of the cross-correlation terms of "A" and "B" do not cancel. Therefore, care must be taken to

insure that there is no cross-talk between the "A" and "B" transmitters and receivers. Hence a transmitter-receiver combination is required for both the "A" codewords and for the "B" codewords. The fields-of-view of these transmitter-receiver pairs must not overlap; i. e., the "A" and "B" channels must be spatially orthogonal. If not spatially orthogonal, the "A" and "B" codewords must be spatially and temporally coded so that no crosstalk occurs between the "A" and "B" channels. An example of the spatial-temporal coding is given in the next chapter.

The CP code requires two transmitters, and thus if each codeword has as many chips as a PN codeword, the received energy per pixel for the CP coding scheme would always be twice that of the PN coding scheme. In order to make comparisons between PN and CP results, the CP code will be

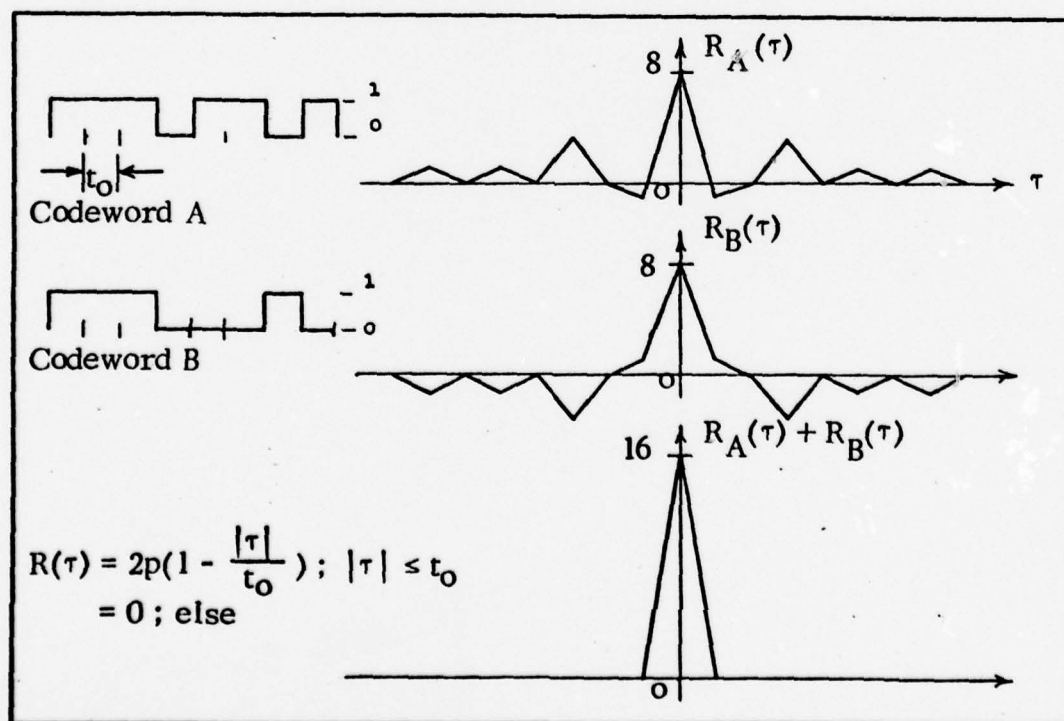


Fig 9. Autocorrelation of a Totally Orthogonal Complementary Pair

required to have half as many chips per word as the PN code, or it must have twice the scan rate (half the dwell time) of that for the PN code. Thus the performance results are normalized to the same total energy per pixel.

The mean square bandwidth may be shown to be

$$B_{CP}^2 \cong \frac{8}{\tau_o^2} \quad (69)$$

The output power has the same form as Eq (65) and, therefore, the detector current signal energy is the same as that given by Eq (66)

$$E_{CP-BPF} = \frac{\beta^2 P_d^2 \tau_d}{4} = \frac{\beta^2 P_d p t_o}{4} \quad (70)$$

$$= 2E_{PN-BPF} \quad (71)$$

where p is the total number of chips in both A and B. The mean square bandwidth and energy for PN and CP codes are approximately the same, and thus it was Eqs (64), (66), and (67) that were used to calculate the performance for pulse coding schemes in the previous section.

Closed-Loop Estimators. Closed-loop estimators are quite different from one-shot matched filters because they employ feedback. The estimator input is compared to a locally generated replica of the signal and an error voltage is generated. The error signal is used to drive the time base for the local reference in the appropriate direction to decrease the error. Closed-loop estimators may be used for both digital and sinusoidal signals. The closed-loop estimator for pulse code modulation

would require many codewords to slide through the filter before the error could be made small. However, the performance of the laser line scan system for pulse code modulation has been shown to be best when the codewords are equal to the dwell time. Therefore, closed-loop estimators would not be practical for this system when pulse code modulation is used.

If RF sinusoidal intensity modulation is used, there would typically be many cycles of the sinusoid in a dwell time. In this case, a closed-loop matched filter is practical. The best known closed-loop matched filter is the phase locked loop (PLL). If

$$y(t) = A \cos(\omega_0 t + \theta) + n(t) \quad (72)$$

then it can be shown that the ML estimator for phase is

$$\int_0^T y(t) \sin(\omega_0 t + \hat{\theta}_{ML}) dt = 0 \quad (73)$$

and may be realized by the PLL below (Fig 10) (Ref 8: 407-409). The CR bounds for the performance of a PLL estimator and direct detector are given by Eqs (55) - (58). From Eq (57) the range ambiguity for sinusoid modulation is

$$R_{amb} = \frac{c}{2f_m} \quad (74)$$

Background Noise Considerations. For high quality, cooled detectors, the noise rate function is given by

$$\lambda_n = \lambda_b + \lambda_d \approx \lambda_D \quad (75)$$

where

$$\lambda_b = \beta P_b \quad (76)$$

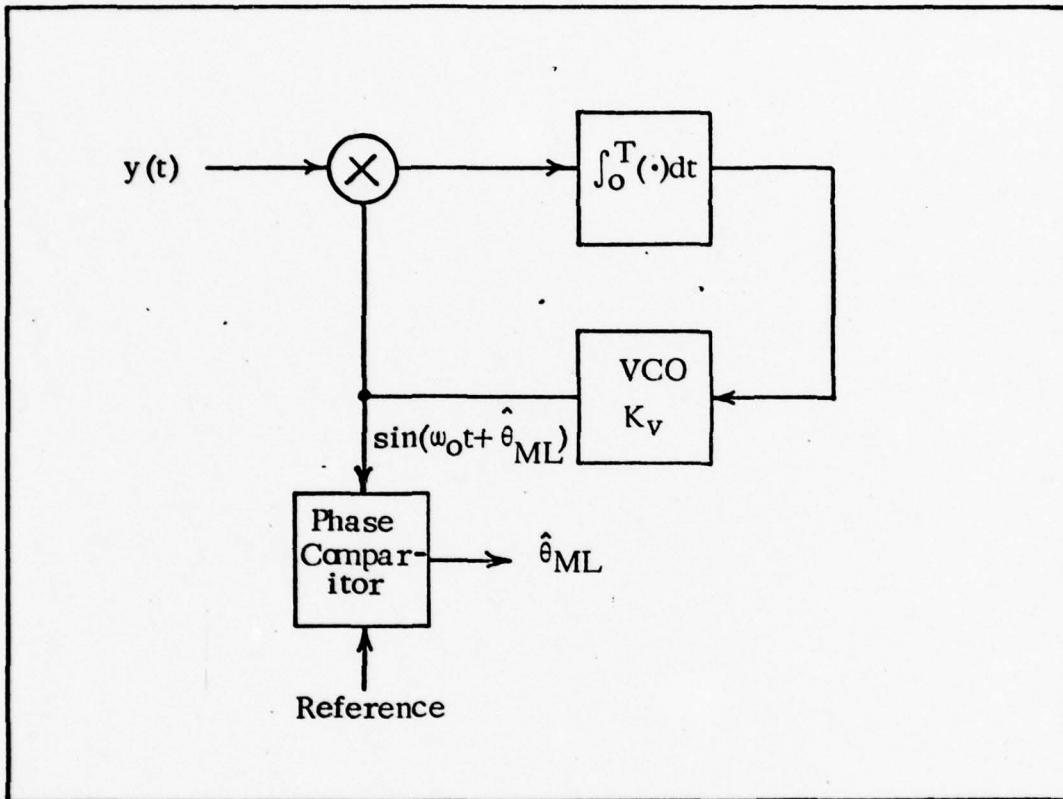


Fig 10. ML Estimator for Phase

P_b is the detected background noise power and may be shown, assuming a Lambertian reflectance target, to be given by

$$P_b = \frac{\rho}{\pi} E_{s,\lambda} t_r \frac{A_r}{r^2} \Delta\lambda A_f \text{ (daytime operation)} \quad (77)$$

where:

$E_{s, \lambda}$ = solar spectral irradiance (watts/cm²-μm)

t_r = transmission of receiver optics and atmospheric path

$\Delta \lambda$ = optical filter bandpass (μm)

A_r = area of receiver optics (cm²)

A_f = area on ground subtended by receiver FOV (cm²)

r = range (cm)

(Ref 12: Chap 5, p. 45). Likewise P_d may be shown to be assuming matched transmitter and receiver FOV's

$$P_d = \frac{P_t}{\pi} \frac{A_r}{r^2} t_t \cos \theta \quad (78)$$

where P_t is the transmitter power, t_t is the transmission of the combined transmitter and receiver optics and two way atmospheric path, and θ is the instantaneous scan angle with respect to the pixel surface normal vector.

The signal-to-noise rate function ratio is given by

$$\frac{\lambda_s}{\lambda_b} = \frac{\rho \beta P_d}{\beta P_b} = \frac{P_t t_t \cos \theta}{E_{s, \lambda} t_t \Delta \lambda A_f} \quad (79)$$

If $P_t = 1$ watt, $t_t/t_r \approx 1$, $\theta = 45^\circ$, $E_{s, \lambda}(.85 \mu m) = 0.007$ watt/cm² - μm

(Ref 13: Chap 6, p. 2), $\Delta \lambda = 0.01 \mu m$, and $A_f = 2090$ cm² (18 inches by 18 inches), then $\lambda_s/\lambda_b \approx 0.48$ and the background noise limited approximation is fairly good for daytime operation. The spectral irradiance

from the moon and stars and the blackbody irradiance of the earth are several orders of magnitude lower than the solar spectral irradiance. Therefore, for nighttime operation, the signal shot noise limited Poisson regime is a good approximation.

III. Spatial and Temporal Coding Analysis

Introduction

In Chapter II it was shown that both the range and reflectance performance variances are inversely proportional to the detected signal energy (Eqs (38) - (41)). There are two practical ways to increase the detected signal energy. The first way would be to use a more powerful laser source. This would require using one of the bulkier, heavier and more fragile solid state or gas lasers. The second, and more attractive, way would be to use more than one GaAs laser diode source. The rest of this chapter will be devoted to investigating methods of temporal coding and spatially scanning N GaAs laser sources to achieve an optimum laser line scan system.

Combining N Source Outputs. The first question that comes to mind when discussing the use of N sources is "Why not use a square $n \times n$ array to form one scanning beam which will be detected by one scanning receiver?", where $n \times n = N$. There are two primary reasons why this is not feasible. The first has to do with thermodynamics; it is very hard to heat sink and cool an array evenly. The diode lasers at the center of the array will be much hotter than those on the outside edge of the array and might be destroyed from thermal effects. The second reason has to do with optics; only one element of the array would be on the optical axis. It is possible to focus the output beam of all of the elements onto one pixel at a given range. However, as soon as the

range changes, the individual beams will no longer be focused on the same pixel and there will be interpixel crosstalk (noise). A solution might be to use fiberoptics to combine the output of N laser diodes. Each diode could be physically mated to an optical fiber which would feed into a star coupler. A single optical fiber out of the star coupler could then be placed at the effective focus of the system optics. Unfortunately, the laser diode to optical fiber junction has a transmission loss on the order of 10db, much too high to be practical.

The major part of this chapter will be devoted to investigating various ways of using N laser sources to simultaneously interrogate or illuminate N different pixels to improve the overall system performance. In order to gain the full advantage of such a multiple source system, the N transmitter-receiver pairs (or channels) must not interfere with each other. This is easily achieved when using pseudo-noise (PN) code modulation. Even if the same signal energy from source m falls into the field-of-view of detector n , the amount of interpixel crosstalk will be minimal so long as the adjacent source modulating signals, $s_m(t)$ and $s_n(t)$, are very nearly temporally orthogonal (zero cross-correlation). Since the autocorrelation of a PN code is $-1/p$ everywhere $\tau \neq 0$, the nearly temporally orthogonal condition can be achieved by cycling the PN codeword transmitted by source n from that transmitted by source m by an amount greater than the maximum expected interpixel delay $\Delta\tau$. The maximum cross-correlation between $s_m(t)$ and $s_n(t)$ will

then never be more than $-1/p$. Unfortunately, complimentary pair (CP) code modulation is not orthogonal; and therefore, interpixel crosstalk may not be minimized by cycling the codewords of adjacent sources. In the CP code modulation case, interpixel or interchannel isolation must be achieved by making the channel-to-channel transmitter-receiver pair fields-of-view (FOV) spatially orthogonal, i.e., the pixel subtended by the FOV of transmitter-receiver pair m must not overlap the FOV of transmitter-receiver pair n . The N channels may also be made temporally orthogonal by using a sinusoidal modulation of a different frequency for each channel. However, Eqs (55), (56) and (74) reveal that the performance and ambiguous range would vary from pixel to pixel. Thus, for sinusoidal modulation, a better method would be to modulate all N sources with the same frequency sinusoid, and again rely on spatial orthogonality of the transmitter-receiver FOV's to achieve inter-channel isolation.

Constraints. The performance of the various spatial-temporal coding combinations presented in this chapter will be expressed using the parameters for a one source line scan system (Fig 11). It will be assumed that the transmitter and receiver fields-of-view are matched, i.e., subtend the same ground area (a pixel) and are spatially orthogonal from channel to channel. The number of pixels per scan line will be a fixed integer

number q . Except for the complimentary pair (CP) pulse code modulation case, the dwell time will be τ_d sec per pixel. In order to insure

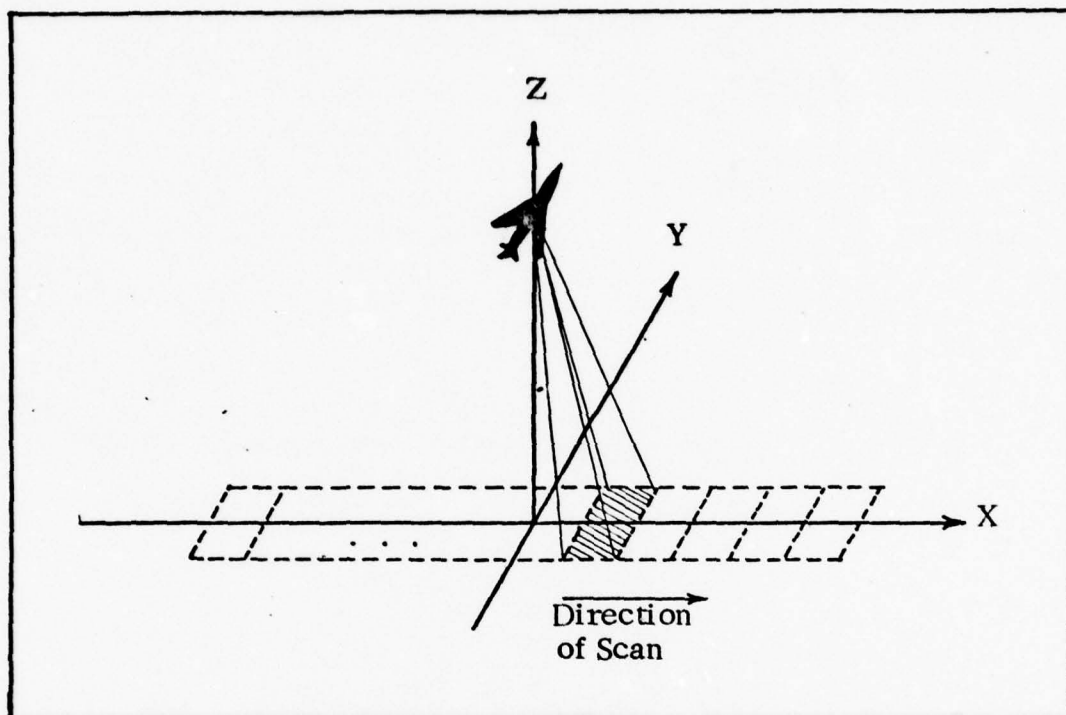


Fig 11. One Source Laser Line Scan System

the same energy per pixel, the two sources required for CP code modulation will each have dwell times of $\tau_d/2$. The period of the scanline is T_s sec where $T_s = q\tau_d$. The total number of sources will be N , whether they are arranged in parallel, series, or a $m \times n$ array where $m \times n = N$. By expressing the performance of each spatial-temporal combination in these common terms, performance comparisons can be easily made in Chapter IV. Since Eqs (38) - (41) indicate that the signal shot noise regime performance is improved in the same way as the background noise

limited regime performance as the signal energy per pixel is increased, only the background noise limited performance of each spatial-temporal combination will be analyzed.

N Sources In Parallel, Pulse Code Modulation

The first spatial-temporal code to be considered places N sources in parallel and uses pulse code temporal modulation. The scanner sweeps out N parallel, contiguous strips along the ground (Fig 12). This configuration can be scanned two different ways. Each will be analyzed below, first using pseudo-noise (PN) pulse code modulation, and then using complementary pair (CP) pulse code modulation.

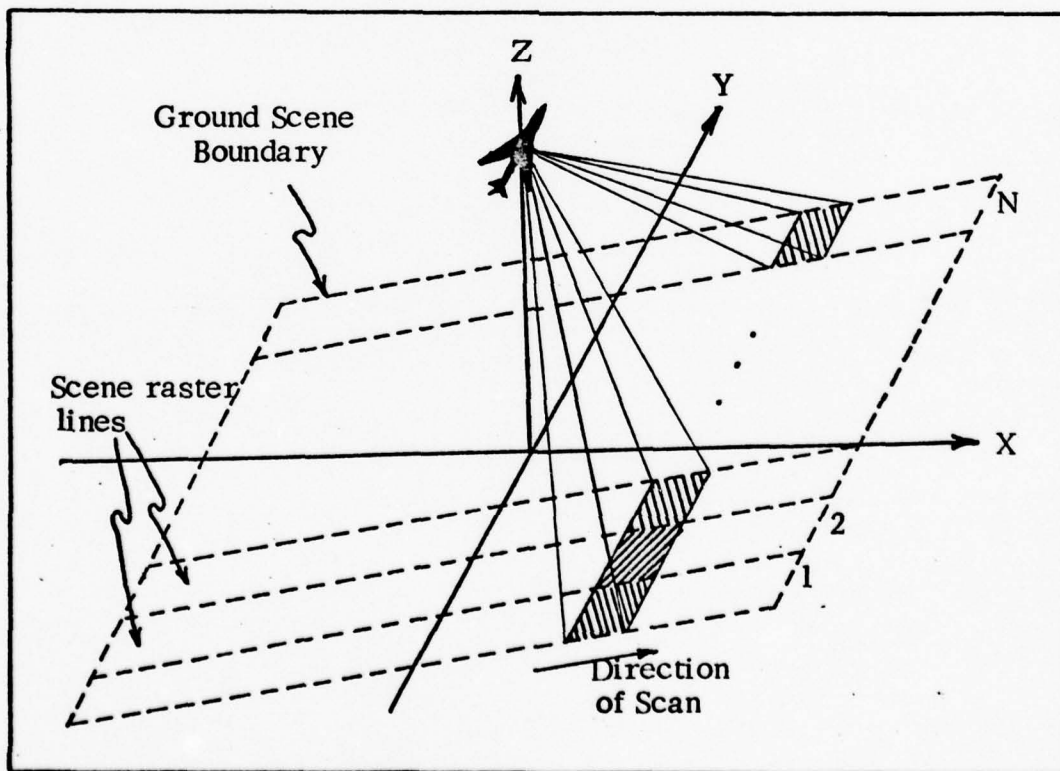


Fig 12. N Sources in Parallel

Slow Parallel Scan, PN Code. Let the N sources be arranged in a parallel scan configuration and be temporally modulated by a PN code. Since N strips are swept out instead of one, the scanner may be swept at $1/N$ the sweep rate required of the single source system and still cover the entire area. Reducing the scan rate causes the strips swept out along the ground to be diagonal, not perpendicular, to the aircraft ground track. This should not pose a serious problem, however, because any processor sufficiently sophisticated to provide cueing will be capable of de-skewing the scene raster lines.

Slowing down the scan by a factor of $1/N$ is equivalent to increasing the dwell time, and consequently the energy, per pixel by N times. The expressions for the range and the reflectance mean square error for each receiver may be found by replacing τ_d with $N\tau_d$ in Eqs (50) and (51), resulting in

$$\sigma_{\tau}^2 \geq \frac{1}{N} \cdot \frac{c^2 \lambda_n t_o^2}{8 \rho^2 \beta^2 P_d^2 \tau_d} = \frac{c^2 \lambda_n t_o}{8 \rho^2 \beta^2 P_d^2 N p} \quad (80)$$

$$\sigma_{\rho}^2 \geq \frac{1}{N} \cdot \frac{2 \lambda_n}{\beta^2 P_d^2 \tau_d} = \frac{2 \lambda_n}{\beta^2 P_d^2 N p t_o} \quad (81)$$

Thus, both the range and the reflectance mean square errors are reduced by a factor of N . From Eq (80), it can be seen that in order to realize the improvement in range estimation performance, the pulse codeword length must be increased by a factor of N ; i.e., the number of chips per codeword must be Np . Increasing the chip duration t_o so that $N\tau_d = p t_o$ will not improve the range estimation performance.

The maximum unambiguous range is proportional to the codeword period, from Eq (63), and becomes

$$R_{\text{amb}} = \frac{cN\tau_d}{2} \quad (82)$$

Therefore reducing the sweep of the scanner also improves the maximum unambiguous range by a factor of N.

Fast Parallel Scan, PN Code . The PN code temporally modulated parallel scanner system may also be swept at the same rate as the single source system, thereby scanning each pixel N times. The dwell time, and consequently the energy per source per pixel, is the same as for the one source system. However, if the signal energy received by each receiver from a given pixel is somehow combined before making the range and reflectance estimates, then the signal energy per pixel is again increased by a factor of N. The N signal returns from each pixel may be combined by an appropriate network of matched filters and delay line summers (Fig 13). The range and the reflectance performance is exactly the same as in the parallel scan case and expressions for the error variances are given by Eqs (80) and (81). However, the dwell time and the pulse codeword length are the same as that of the single source system, therefore, the maximum unambiguous range is given by

$$R_{\text{amb}} = \frac{c\tau_d}{2} \quad (83)$$

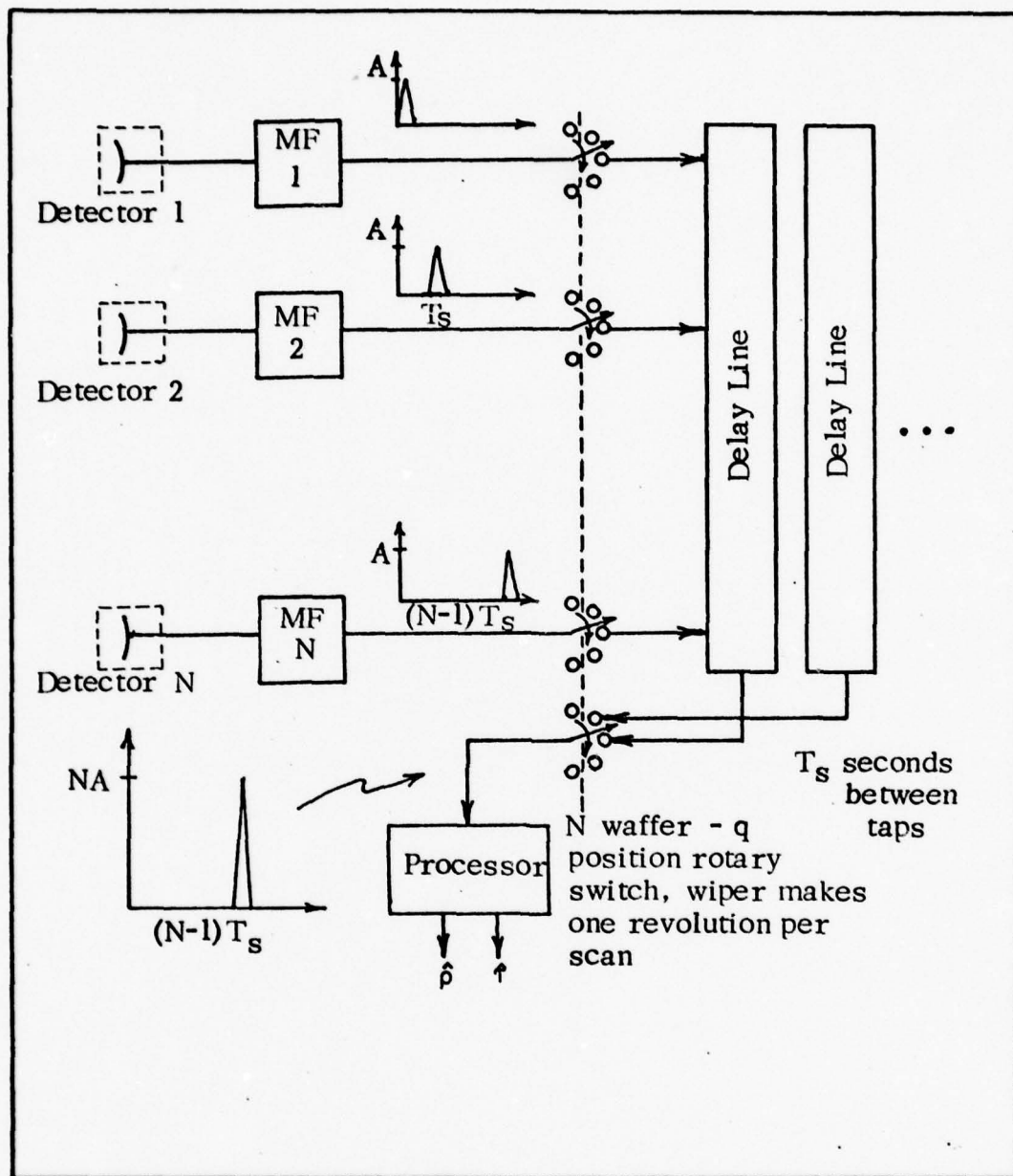


Fig 13. Receiver Configuration for "Fast Parallel Scan - PN Code" System

Besides the shorter unambiguous range, this configuration requires q of the relatively long delay line summers shown in Figure 11, one for each pixel in the scan line. However, it does have the advantage that any differences in individual laser power outputs and individual detector responsivities are averaged out by the delay line summers. Also, the strips swept out on the ground will be much closer to perpendicular to the aircraft ground track than those in the parallel scan case.

Slow Parallel Scan, CP Code. Now consider the N parallel scanning sources temporally modulated with a CP code. Let the first $N/2$ sources transmit codeword "A", the second $N/2$ sources transmit the complimentary codeword "B", and the N sources be scanned at a rate which is $2/N$ that of the one source system scan rate. Each pixel will be scanned twice, first by a source transmitting codeword "A", and then $NT_s/2$ sec later by a source transmitting the complimentary codeword "B", where T_s is the scan period of the single source system. Now, the effective dwell time is $N\tau_d/2$ and each pixel is scanned twice so that the total received signal energy per pixel is again increased by a factor of N . The two signal returns from each pixel may be processed by using a delay line (Fig 14). The performance is exactly the same as in the previous two cases and the expressions for the error variances are given by Eqs (80) and (81). From Eq (63) the maximum unambiguous range is

$$R_{amb} = \frac{c N \tau_d}{4} \quad (84)$$

i.e., $N/2$ times that for the single source system.

This spatial-temporal combination requires $qN/2$ delays, has a skewed scene raster, and only averages responses of two transmitter-detector pairs. It also requires strict spatial orthogonality.

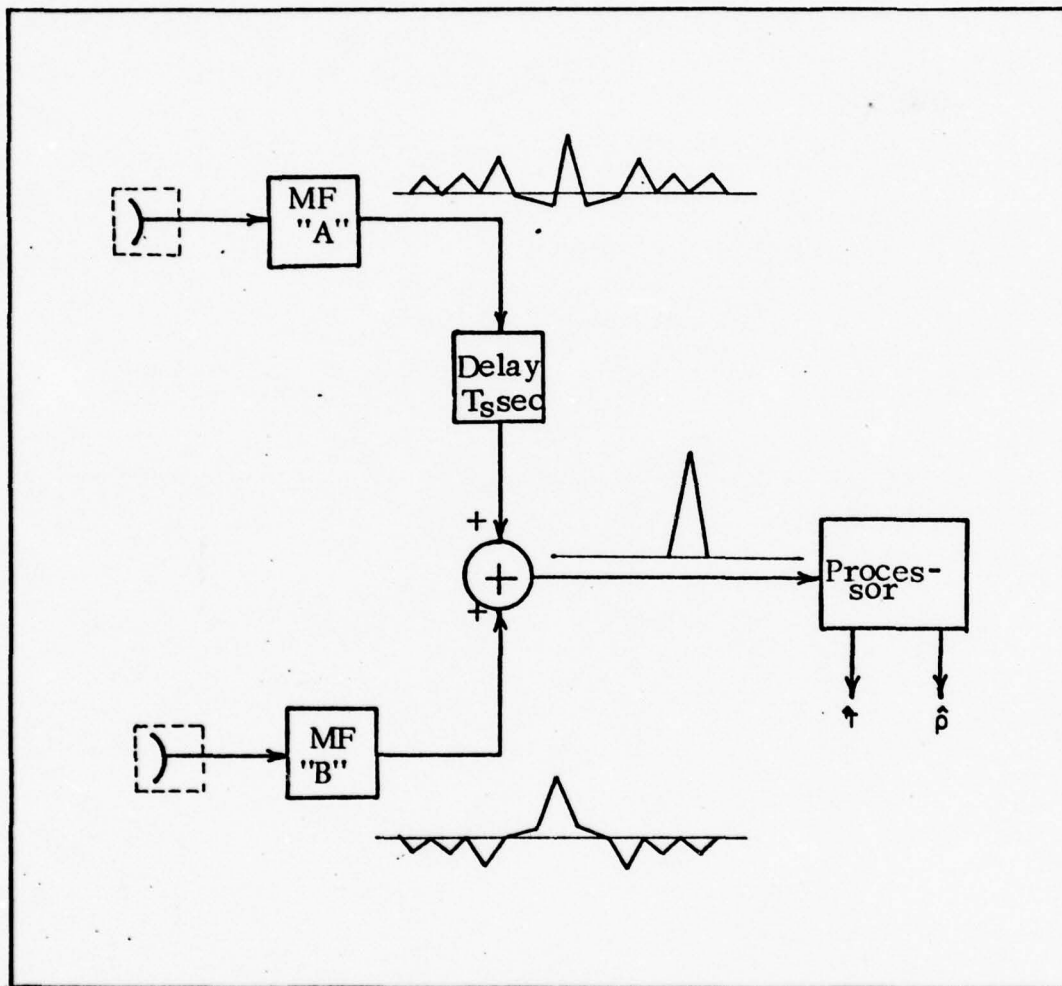


Fig 14. Receiver Configuration for CP Coding

Fast Parallel Scan, CP Code. The N sources may also be scanned at the same rate as the single source system while being temporally

modulated by a CP code. The only difference between this and the PN case discussed above is that one-half of the sources must transmit codeword "A" and the other half must transmit codeword "B". There are several ways this may be done, but one way might be to let all of the odd numbered sources transmit codeword "A" and let all of the even numbered sources transmit codeword "B". The receiver outputs may be combined by using the configuration shown in Figure 11 where all of the odd matched filters are matched to codeword "A" and all of the even matched filters are matched to codeword "B". The performance expressions and unambiguous range are exactly the same as for the "Fast Parallel Scan-PN Code" case and are given by Eqs (80), (81), and (83). The advantages and disadvantages are nearly identical also. This case has the additional disadvantage of requiring N more delays, and has the additional advantage that the CP code is linear and will not be affected by inter-pixel delay differences.

N Sources In Series, Pulse Code Modulation

Another possible spatial-temporal code places N sources in series and uses pulse code temporal modulation (Fig 15). Since only one strip of ground is swept at a time, the scan rate must be the same as that of the single source system in order for the scanned strips to be contiguous. Thus, as in the "Fast Parallel Scan" case, the energy per source per pixel is the same as the single source case; therefore, once

again, all of the receiver outputs must be combined before making range or reflectance estimates. If CP code modulation is used, with alternating codewords "A" and "B", the N receiver outputs may be combined via the

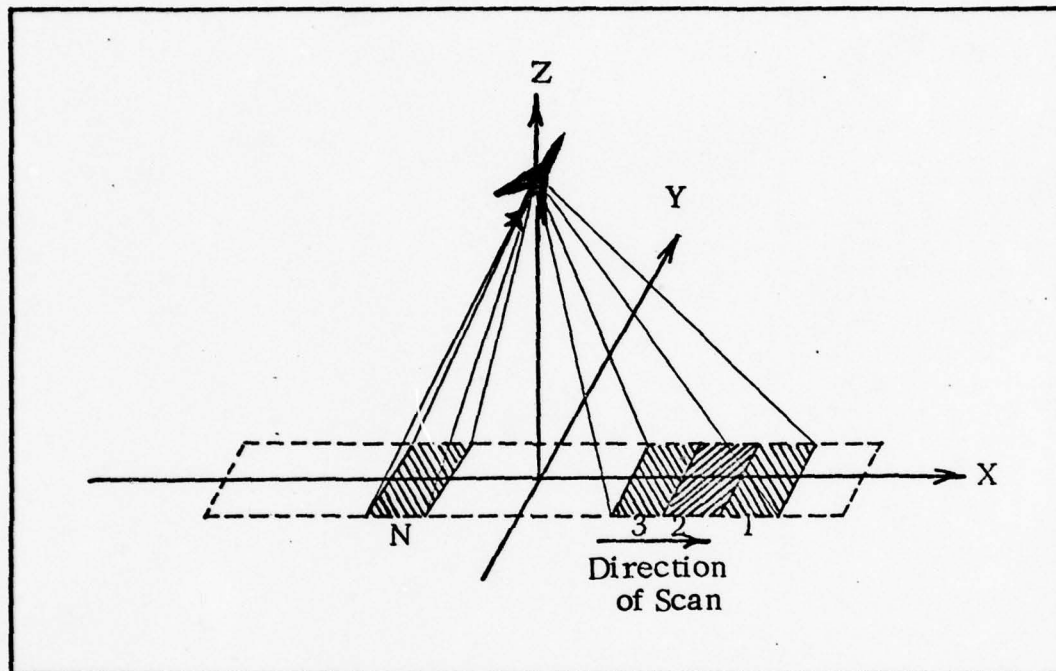


Fig 15. N Sources in Series

receiver configuration shown below (Fig 16). If PN code modulation is used, the matched filters are merely matched to the PN codeword. It can easily be shown that, just as in the parallel scan case, the performance is the same regardless of whether PN or CP code modulation is used, and is equal to that of the parallel scanning systems. Also, since the dwell time is τ_d for the series scan regardless of the type modulation used, the maximum unambiguous range is also the same as that of the single source

system. Thus, the performance expressions and unambiguous range are given by Eqs (80), (81), and (83). This system has one large advantage over the parallel scan systems. In addition to having nearly perpendicular raster lines and averaging out the responses of the different transmitter-detector pairs, only one relatively short delay line summer is required to combine the N detector outputs.

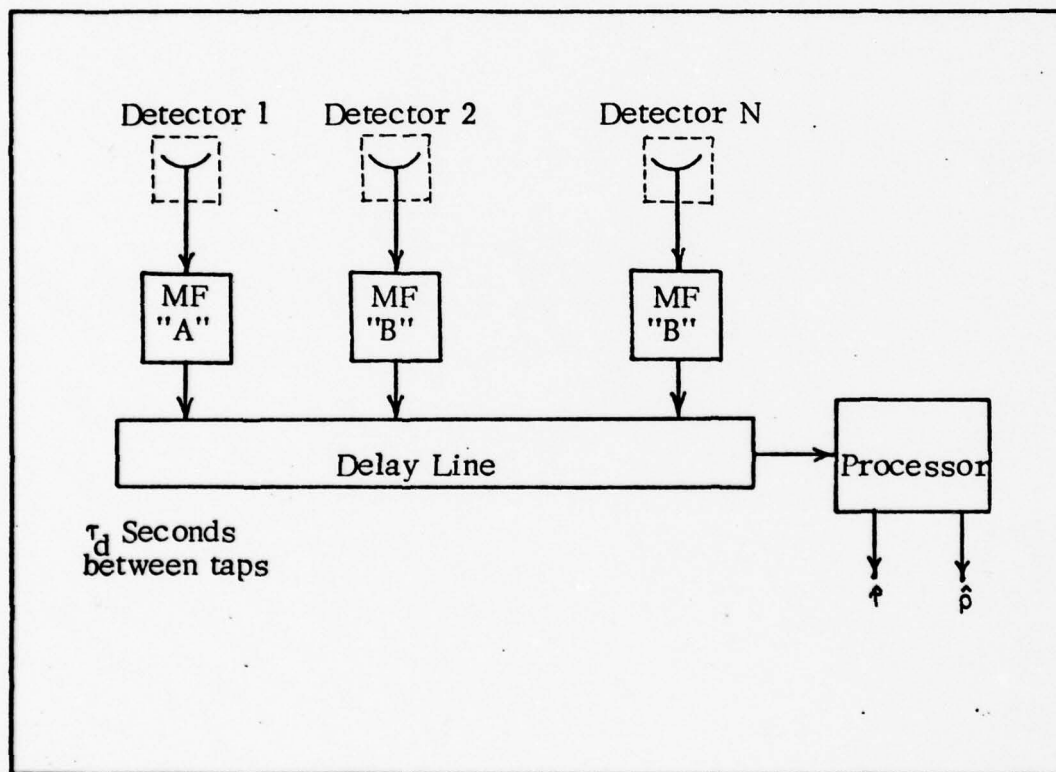


Fig 16. Receiver Configuration for "Series Scan - PC Modulation"

N Sources In An Array, Pulse Code Modulation

It is conceivable that a N source scanner might be configured using a combination of the parallel and series scanning systems and temporally modulated with pulse code modulation. It can easily be

shown that, so long as the total number of sources is N and all of the detector outputs are summed before processing, then the performance of this type system will be exactly that of either the parallel or series scan systems, and will be independent of which type of code, PN or CP, is used.

The major things that will vary with configuration will be the maximum unambiguous range, the complexity of the receiver configuration, the angle of the scene raster lines with respect to the ground track, and the number of transmitter-detector pair responses that are averaged. For an $m \times n$ array, let there be m sources in parallel, and n sources in series. From the discussions above, it is clear that the simplest delay line summer network will be realized if the system is scanned at the "slow" rate of $1/m$ that of the single source system, and no detector outputs are combined. In this configuration, a block of m contiguous strips are swept out, and then the system moves forward and sweeps out another block of m strips adjacent to the first block. Once more the range and reflectance performance expressions are given by Eqs (80) and (81). The dwell time is $m\tau_d$, and thus the maximum unambiguous range is

$$R_{amb} = \frac{c m \tau_d}{2} \quad (85)$$

For this configuration, m delay line summers are required to combine the n detector outputs per scan line. The greatest disadvantage of this

configuration is that an $m \times n$ array of laser diodes, either on one substrate or in an array of individual diodes, is required for the transmitter. The former is unlikely because of the difficulty in cooling the array; and the latter is undesirable due to the bulk and complicated optics involved.

N Sources In Parallel, Sinusoidal Modulation

The N parallel source scan configuration shown in Fig 10 may also be sinusoidally temporally modulated. If the scanner is swept at $1/N$ the rate of the single source system, then the dwell time is once again $N\tau_d$. The expressions for the range and the reflectance mean square errors may be found by dividing Eqs (55) - (56) by N , resulting in

$$\sigma_r^2 \geq \frac{1}{N} \cdot \frac{c^2 \lambda_n}{2\pi^2 f_m^2 \beta^2 P_d^2 \tau_d} \quad (86)$$

$$\sigma_\rho^2 \geq \frac{1}{N} \cdot \frac{8\lambda_n}{3\beta^2 P_d^2 \tau_d} \quad (87)$$

where f_m is the frequency of the sinusoidal intensity modulation of the N sources.

The maximum unambiguous range is given by Eq (74), and is

$$R_{amb} = \frac{c}{2f_m} \quad (74)$$

Note that the performance is inversely proportional to f_m squared where as the range ambiguity, which is independent of dwell time for sinusoidal modulation, is inversely proportional to f_m . Thus, there is a definite

tradeoff between system performance and maximum unambiguous range. For example, if the laser were intensity modulated near its maximum frequency response, say 100MHz, to minimize the range and reflectance errors, the unambiguous range would be 1.5 meters (4.9 feet).

This coding combination will also exhibit the skewed raster lines as in the "Slow Parallel Scan, Pulse Code" cases discussed earlier. Another disadvantage is that any differences in transmitter-detector pair responsivity will not be averaged out as in the fast scanning configuration.

For an implementation of a fast parallel scan configuration or a series scan configuration using sinusoidal modulation, it can be shown that the performance and maximum unambiguous range is just that of the slow parallel scan case. The advantages of the fast parallel or serial scans would be the reduced skewing of the raster lines and the averaging of the N channel responsivities. Unfortunately, these implementations are not practical. As in the pulse code modulation cases above, it would be necessary to coherently combine the N receiver outputs from each pixel before making range or reflectance estimates. The coherent addition of RF frequencies using many fairly long delay lines would be very difficult.

N Sources In Parallel, Multiple Sinusoidal Modulation

Using existing technology, sinusoidal intensity modulation of high powered GaAs laser diodes can be done (Ref 2). For this reason, it is highly desirable to find some kind of sinusoidal temporal modulation

which has a large maximum unambiguous range. One such method is to use two superimposed sinusoids of different, but close, frequencies (Fig 17).

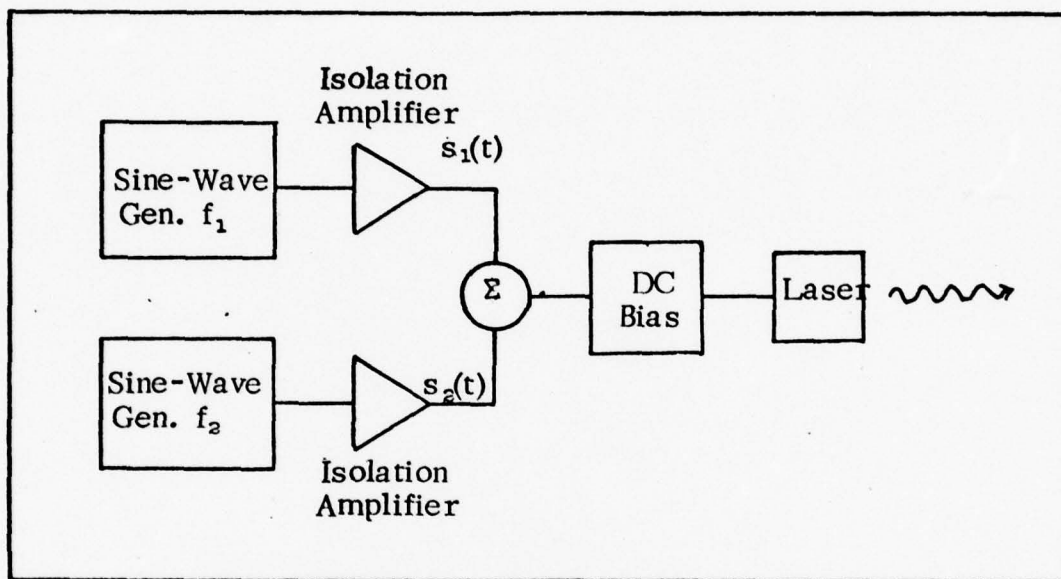


Fig 17. Multiple Sinusoid Transmitter Configuration

If the two sinusoids are given by

$$S_1(t) = \sin(2\pi f_1 t + \phi_1) \quad (88)$$

$$S_2(t) = \sin(2\pi f_2 t + \phi_2)$$

then the range and maximum unambiguous range are

$$R = \frac{c \Delta \phi}{4 \pi \Delta f} \quad (89)$$

$$R_{\text{amb}} = \frac{c}{2 \Delta f} \quad (90)$$

where $\Delta \phi$ is the phase difference between the two received sinusoids and $f_2 = f_1 + \Delta f$ (Ref 14: 106-107). Thus such a modulation scheme has a potential for coarse range measurement with long unambiguous range provided that the standard deviation of Δf is less than f_2 . Fine range resolution measurements can be made by routing the output of a high-pass filter centered at f_2 into a phase locked loop.

The performance of the fine range estimates may be found from Eq (55), which may be expressed as

$$\sigma_r^2 \geq \frac{c^2 \lambda_n}{16 \pi^2 f_2^2 \rho^2 E_s} \quad (91)$$

where E_s is given by Eq (48). Since the laser diodes are assumed to be peak power limited, the vector sum of the two modulating sinusoids may not exceed the laser's peak output power. Therefore, $s(t)$ in Eq (54) becomes

$$s(t) = \frac{\beta P_d}{2} (1 + \frac{1}{2} \sin 2\pi f_1 t + \frac{1}{2} \sin 2\pi f_2 t) \quad (92)$$

Substituting the high-pass filtered output, $(\rho \beta P_d/4) \sin 2\pi f_2 t$, and Eq (48) into Eq (90) yields

$$\sigma_r^2 \geq \frac{2c^2 \lambda_n}{\pi^2 f_2^2 \rho^2 \beta^2 P_d^2 \tau_d} \quad (93)$$

The performance of the reflectance estimates may be found by substituting Eqs (92) and (48) directly into Eq (39) yielding

$$\sigma_p^2 \approx \frac{16\lambda_n}{5\beta^2 P_d^2 \tau_d} \quad (94)$$

Dividing Eqs (93) - (94) by N and then comparing to Eqs (86)-(87) reveals that the effect of splitting the available laser power between two sinusoids to increase range ambiguity by a factor of $f_c/\Delta f$ is to increase the mean square range error by a factor of (4) and the mean square reflectance error by a factor of (1.2).

Temporal Modulation Via Electro-optic Modulators

High power laser diodes have low input impedances and require high drive currents. Thus, narrow pulses are difficult to obtain because the extremely large voltage drops across associated circuit inductances as small as a nano-henry. Since Eq (71) implies that the range performance of pulse code modulation schemes is proportional to the chip width t_o , indirect methods of obtaining narrow intensity pulses are attractive. Temporal intensity modulation may be achieved using electro-optic modulators such as Kerr cells or Pockel cells (Ref 15: 245-268). Gigabit per second modulation rates with 24 volt modulation voltage and 81.5% static transmission for 530nm light have been obtained using Pockel cells (Ref 16).

If the high power GaAs laser diodes are assumed to be unpolarized, then there will be an automatic 3 db power reduction due to the Pockel cell polarization analyzer. Thus, the total through-put would be approximately $0.4 P_t$. Assuming peak power limited laser diodes, the previous pulse

modulation analysis may be used by replacing P_t everywhere by $0.4 P_t$. Thus the range and reflectance rms errors will be 2.5 times larger than the case of identical parameters obtained by direct modulation of the laser diode drive current. However, if the electro-optic modulator is capable of chip widths less than 0.16 that available by direct modulation, then the loss of power will have been overcome, and the electro-optic modulator will provide the best performance. This result is valid assuming that the overall system response is limited by the speed of the transmitter, and not that of the detector.

Temporal Modulation Via Spatial Coding

Another indirect way of generating a pulse at the output of the receiver is to stare at a given pixel with a detector and sweep the transmitted beam from a CW source through the detector field-of-view (FOV). Thus, it is possible to temporally modulate the energy return from a pixel by spatially coding the scanner. The detector output is just the spatial-temporal convolution of the transmitter and receiver FOVs. If the scanning transmitter beam is spatially coded with a given sequence, then the detector's output will look like a pulse code word with the same sequence. This may be accomplished two ways: (1) N-series, spatially coded sources may be scanned $p/2$ times per scan line by a rotating polygonal prism with $p/2$ faces (Fig 18); and (2) N-CW sources in parallel may be scanned by a coded rotating polygonal prism with p faces;

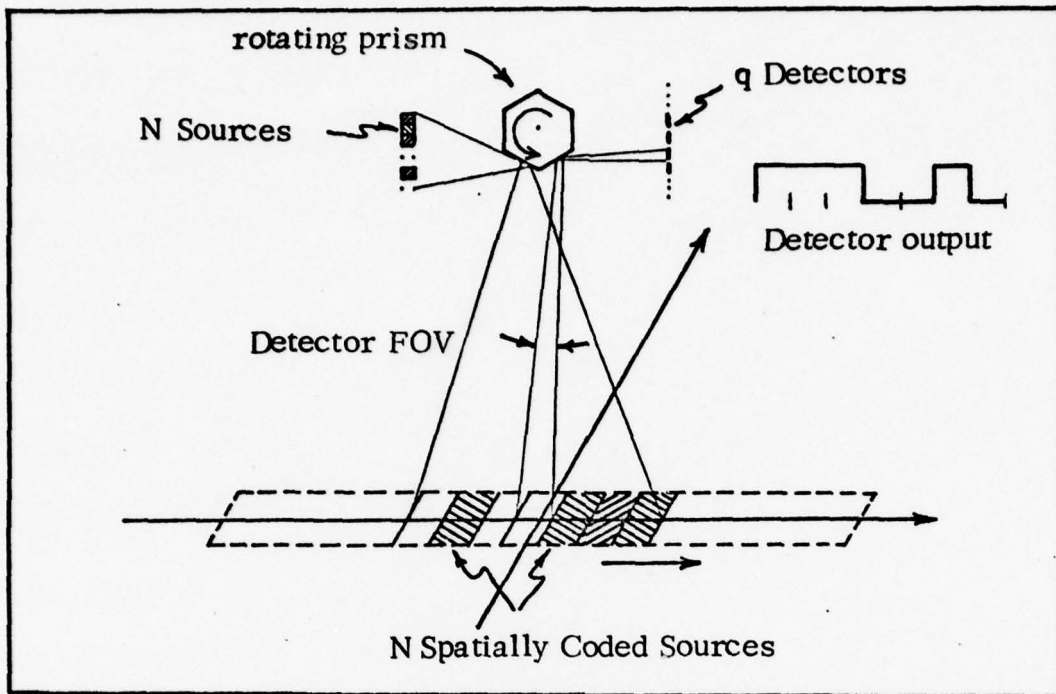


Fig 18. N Series, Spatially Coded Sources

a digital "one" would correspond to a highly polished prism face, and a digital "zero" would correspond to a rough prism face (Fig 19). The length of the codeword is a $2N$ chips for the first case and p chips for the second case. So long as the number of sources, the number of sides of the polygon, and the chip duration (dwell time) t_0 are such that $N\tau_d = Npt_0$ then the rms errors for the range and reflectance estimates will be given, once again, by Eqs (80) and (81), and the unambiguous range will be given by

$$R_{amb} = cNt_0 \quad (95)$$

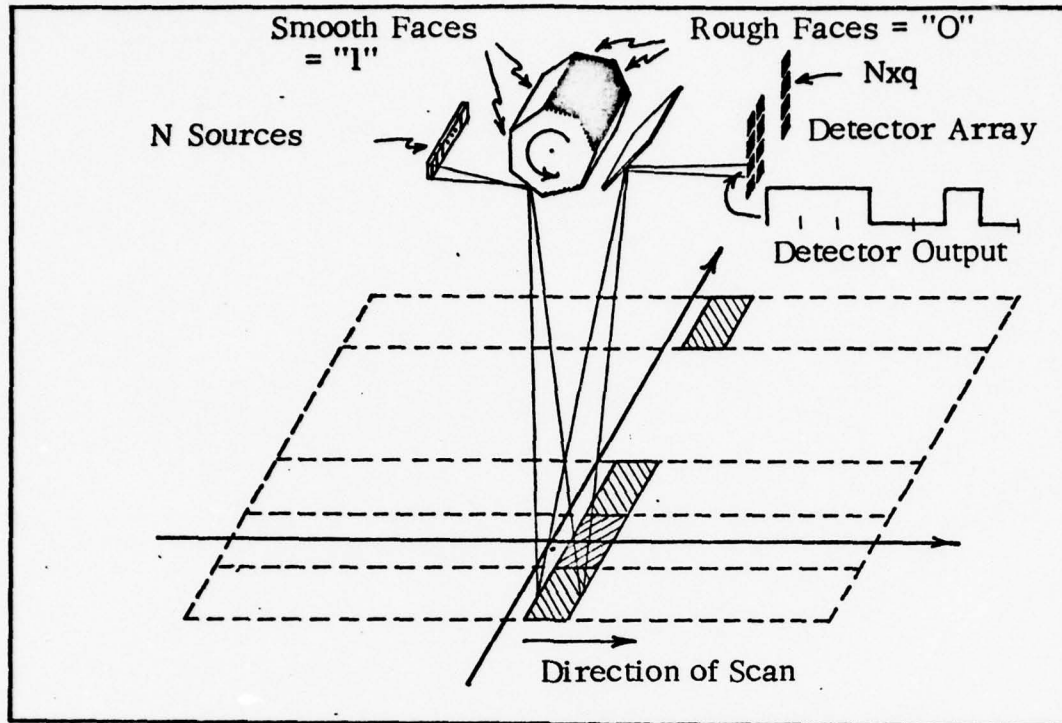


Fig 19. N Parallel, Spatially Coded Transmitter Beams

for N series, spatially coded sources, and by

$$R_{amb} = \frac{cpt_0}{2} \quad (96)$$

for N sources in parallel. Hence, if t_0 can be made shorter via spatial coding, then the performance will be improved. The price that is required for this improvement is the need for ultra-fast scanner rotation rates, large numbers of detector elements, and complicated optics. It should be noted that a beam splitter would be required to sample the transmitted beam in order to obtain a reference from which to measure delay. A very small amount of optical signal (from the beam splitter) would be detected and processed by the matched filter. The time between the

occurrence of a peak at the matched filter output due to the reference and the occurrence of a peak due to the reflected signal is the delay estimate τ .

Hybrid Spatial and Temporal Coding

In an effort to increase the bandwidth of the intensity modulation, a transmitted laser beam may be both temporally modulated and spatially coded, thereby producing a hybrid modulation at the detector output. If pulse code temporal modulation is used and the codeword period is longer than a dwell time, the effect will be to modulate or "gate" the temporal modulation with the spatial code (Fig 20). Thus, if the autocorrelation properties of the PN or CP codes are to be preserved, the codeword duration must be less than or equal to the dwell time. Hence there is no advantage to gating a pulse code temporal modulation via spatial coding.

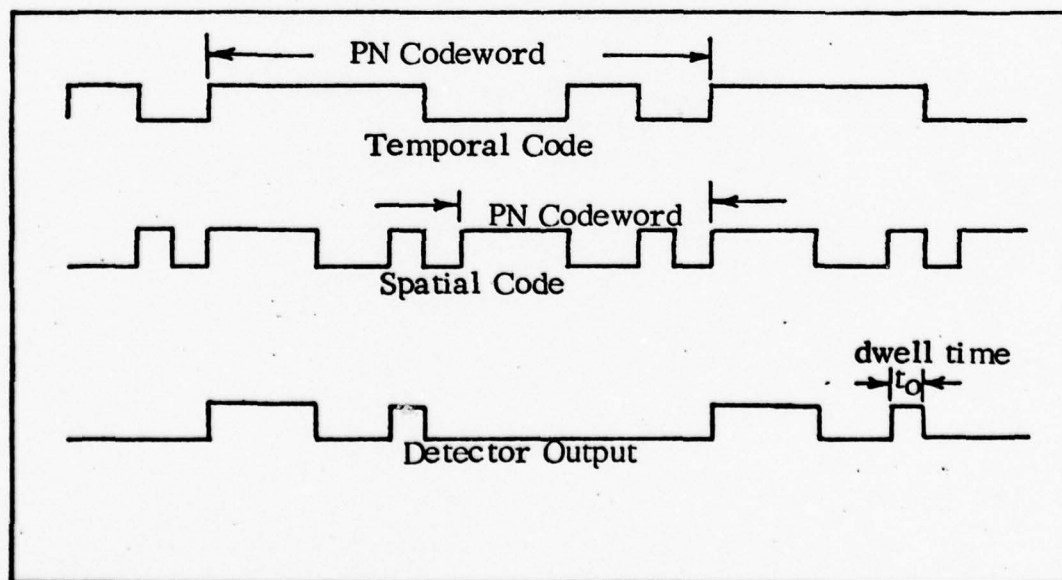


Fig 20. Hybrid Spatial-Temporal Code

However, if the source is temporally modulated with a sinusoid, the result of spatial coding will be to On-Off-Key (OOK) the sinusoid. If the spatial code is a pulse code, then the output of the photodetector is a pulse coherent pulse code (Fig 21). Thus, if a phase locked loop (PLL) can achieve phase lock by the end of the pulse codeword, it may then be used to make range and reflectance estimates; and the pulse codeword may be coherently detected and used to resolve the range ambiguity of the sinusoid.

Recall that the reason for considering the spatial coding in the first place was to obtain a way of creating pulses with pulsewidths smaller than could be achieved via direct modulation of the laser diode drive current.

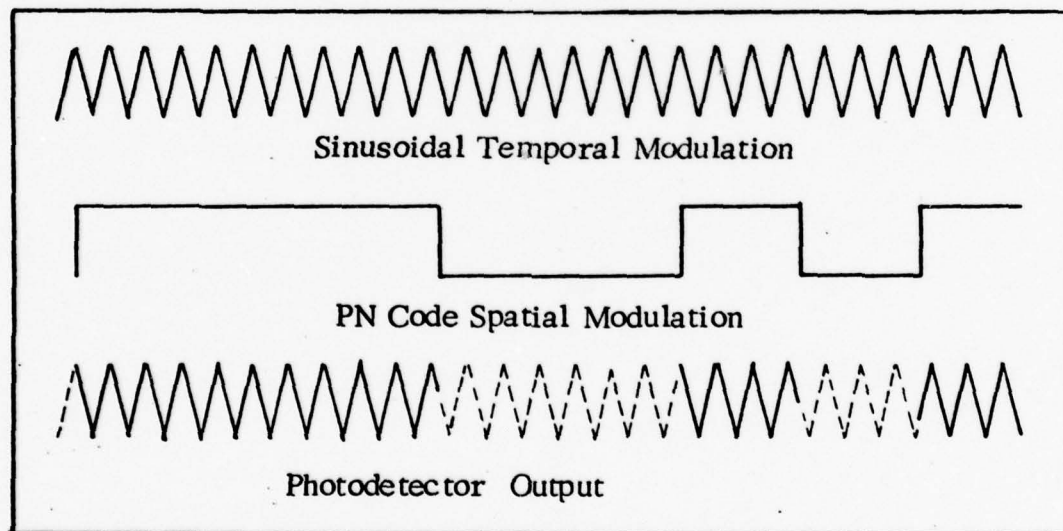


Fig 21. On-Off-Keying Via Hybrid Spatial-Temporal Coding

The OOK sinusoidal modulation does not require narrow chips. In fact, the chips must be long enough for many cycles of the sinusoid to fit inside

a chip so that the PLL can achieve phase lock. Hence, there is no advantage to gating sinusoidal temporal modulation via spatial coding. The disadvantages include high scanner rotation rates, large numbers of detector elements, and complicated optics.

N Sources in Parallel, OOK Sinusoidal Modulation

Each source of the N parallel source scan configuration shown in Fig 12 may be OOK sinusoidally temporally modulated by direct modulation of the laser source drive current (Fig 22). The range and reflectance estimates for each of the N detectors may be made via the receiver configuration

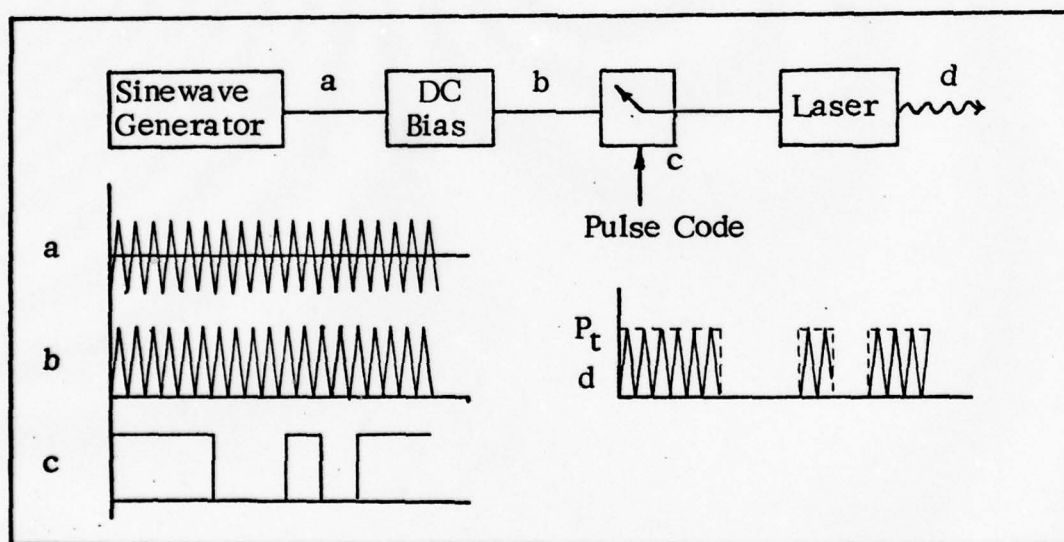


Fig 22. Transmitter Configuration for OOK

below (Fig 23). The voltage controlled oscillator (VCO) constant K_v (see Fig 16) must be small in order for the PLL to acquire and maintain phase lock with OOK sinusoidal input. Thus, two PLLs are alternated

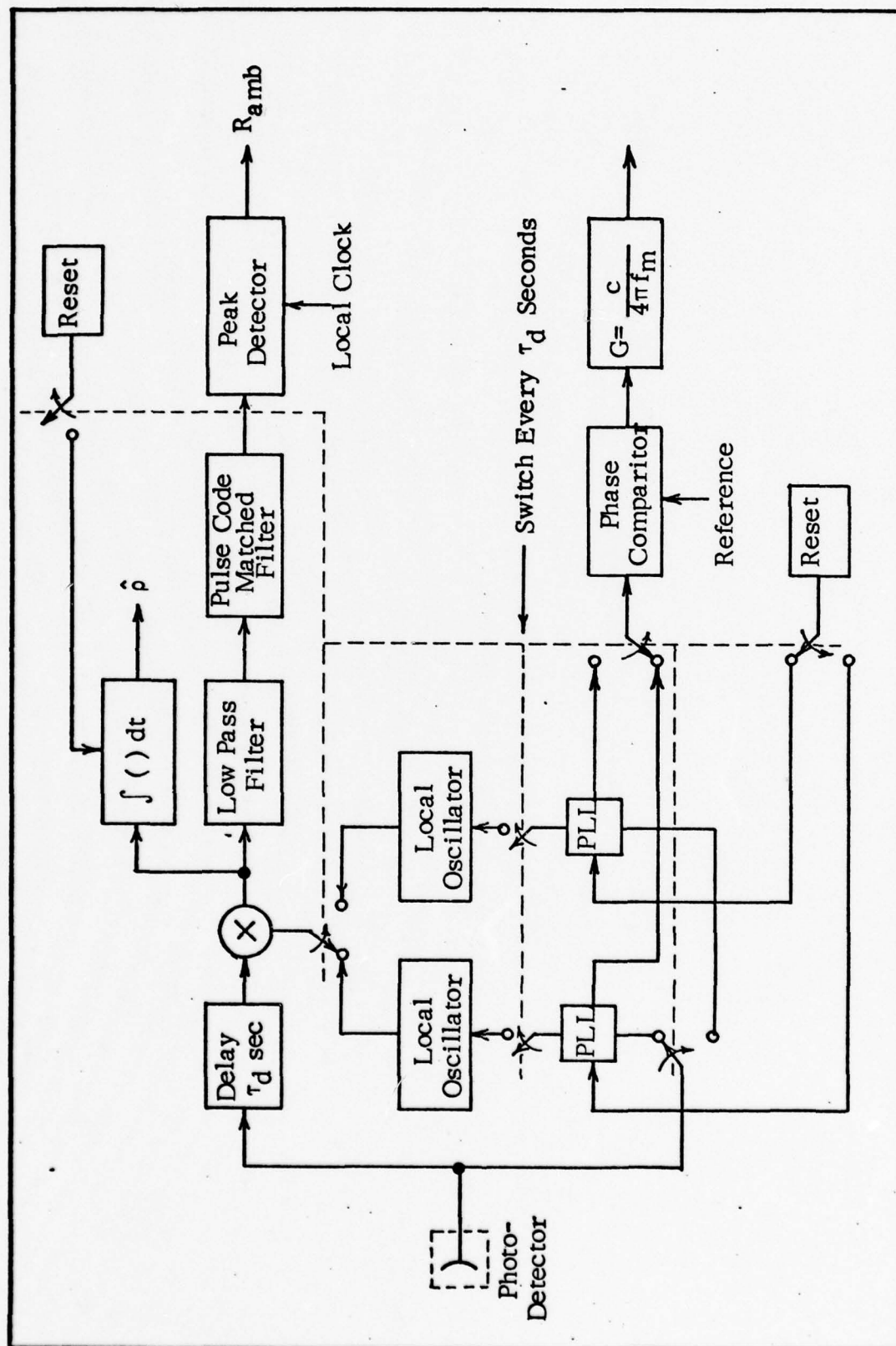


Fig 23. Receiver Configuration for OOK Modulation

to make the phase estimates. A local oscillator samples and "remembers" the phase and frequency of the PLL at the end of a dwell time (codeword period). The local oscillator output is then used to coherently detect the delayed OOK pulse codeword. Each PLL is reset before being used to make phase estimates for a particular pixel.

The Cramer Rao performance bounds for the mean square range and reflectance errors may be found from Eqs (86) and (87). The OOK with a pulse code has the effect of cutting the illumination time of each pixel in half, thereby reducing the signal energy out of the detector by one-half; thus, replacing τ_d by $\tau_d/2$ in Eqs (86) and (87),

$$\sigma_r^2 \geq \frac{1}{N} \cdot \frac{c^2 \lambda_n}{\pi^2 f^2 \rho^2 \beta^2 P_d^2 \tau_d} \quad (97)$$

$$\sigma_\rho^2 \geq \frac{1}{N} \cdot \frac{16 \lambda_n}{3 \beta^2 P_d^2 \tau_d} \quad (98)$$

The resulting mean square errors for range and reflectance are 2 times larger than for sinusoidal modulated sources.

The input to the pulse code matched filter is

$$\begin{aligned} \text{Low Pass} \quad & \{ \rho \beta P(t) [1 + \cos(\omega_m t + \theta)] \cos(\omega_m t + \hat{\theta}) \} \\ & = \rho \beta \frac{P(t)}{2} \end{aligned} \quad (99)$$

where $P(t)$ is given by Eq (65) with P_t replaced by P_d .

Therefore, the signal energy available to the matched filter is just one-fourth what it was for the pulse code modulation case; thus

$$\sigma_{R_{amb}}^2 \geq \frac{c^2 \lambda_n t_0}{2 \rho^2 \beta^2 P_d^2 p} \quad (100)$$

A conventional, though arbitrary, measure of range resolution is that two target echoes must be separated by at least the full width at half maximum of the matched filter output. Similarly, in order for the pulse code to help resolve the sinusoidal range ambiguity, a logical, though arbitrary, requirement is that

$$2 \sigma_{R_{amb}} \geq \frac{c}{2f_m} \quad (101)$$

Substituting Eq (100) into Eq (101) and solving for t_0 yields

$$t_0 \geq \frac{\rho^2 \beta^2 P_d^2 p}{8 \lambda_n f_m^2} \quad (102)$$

For example, if the sinusoidal modulation frequency is 100 MHz, $\rho \beta P_d = 0.1 \lambda_n$ (background noise limited case), $P_b = 10^{-8}$ watts, $\beta = 2.5 \times 10^{18}$ joules⁻¹ and $p = 13$, then t_0 must be less than or equal to 41 nsec, approximately four times the period of the sinusoid. As the signal-to-noise ratio and/or the number of chips p increases, the longer t_0 may be while still meeting the requirement expressed by Eq (102). Chips widths of this order-of-magnitude should be relatively easy to achieve, especially if the

laser diode and associated drive circuitry has a natural resonant frequency near f_m , which is usually the case.

The maximum unambiguous range for the OOK sinusoidal modulation is the same as for the N Sources in Parallel, Slow Scan, PCM case, and is given by Eq (82)

$$R_{amb} = N \frac{c\tau_d}{2} = \frac{Nc\tau_{pt0}}{2} \quad (82)$$

It is not practical to try to implement the OOK sinusoidal modulation with a fast, parallel source scan configuration, or with a serial source scan configuration. This is because the signal energy must be above a certain threshold for a PLL to acquire and maintain phase lock. Thus, the output OOK sinusoidal modulation from the N individual receivers for each pixel must be coherently combined before being applied to the PLL. As stated earlier, the coherent addition of many RF frequency signals would be extremely difficult.

q - Staring Sources and Detectors, Pulse Code Modulation

A non-scanning sensor configuration may be realized with q source-detector pairs (one for each pixel of the scan line). Although this scheme requires more sources than the previous cases, it has the advantage of no moving parts; the staring source-detector pairs swept out the scene as the aircraft moves forward (Fig 24). The effective dwell time is just the time

it takes for the aircraft to move forward a pixel width, and is q times the dwell time for the single source, τ_d . The length of the pulse codeword may now be quite long to provide very good estimation performance. For pulse code modulation, either PN codes with length $q\tau_d$ or CP codes with two words of length $q\tau_d/2$, the expression for the range and the reflectance mean square error become

$$\sigma_r^2 \geq \frac{1}{q} \cdot \frac{c^2 \lambda_n t_0^2}{8 \rho^2 \beta^2 p_d^2} \quad (103)$$

$$\sigma_\rho^2 \geq \frac{1}{q} \cdot \frac{4 \lambda_n}{\beta^2 p_d^2 \tau_d} \quad (104)$$

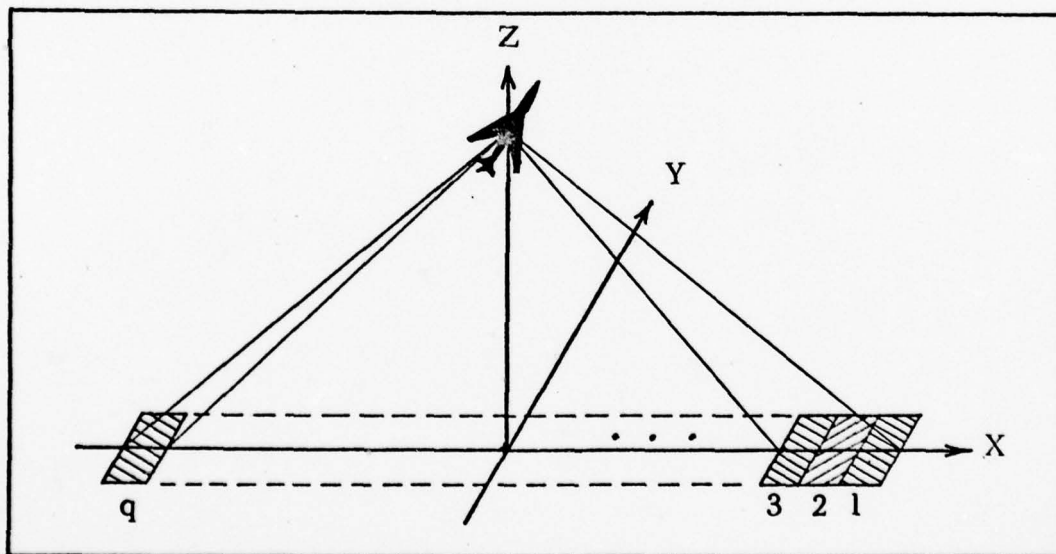


Fig 24. q - Staring Source-Detector Pairs

The maximum unambiguous range becomes

$$R_{\text{amb-PN}} = q \frac{c \tau_d}{2} \quad (105)$$

for PN code modulation, and

$$R_{\text{amb-CP}} = q \frac{c\tau_d}{4} \quad (106)$$

for complimentary code modulation. Comparing these results with those given by Eqs (71) - (73) and (75) for N pulse code modulated sources, the range and the reflectance mean square errors and the maximum unambiguous range are all improved by a factor of q/n . The price required for this improvement is q/n times more source-detector pairs and the inability to average out the differences in source-detector responsivities.

q - Staring Sources and Detectors, Spatial and Temporal Modulation

The q-staring sources described in the previous section may be spatially coded, or may be scanned conventionally, by electronic means. In order to separate the return from each pixel, it is required that the q source-detector pairs be spatially or temporally orthogonal, or both. Spatial orthogonality may be hard to achieve using GaAs lasers for sources because they have rather large beam divergences. Thus, in order to reduce channel-to-channel cross-talk as much as possible, it may become necessary to restrict the source modulation so that no adjacent sources transmit simultaneously. Such a scheme is described below for CP code modulation.

Suppose the projection of the beam is made smaller than the pixel, and each pixel is divided into five intervals and the q-element linear array is divided into 5 different element groups (Fig 25). Each element of a

given group, group 1 (all of the sources labeled "1" in Fig 25) for instance, are separated by four elements from the other four groups. All of the elements of group 1 simultaneously transmit codeword "A" of the CP code, and then transmit codeword "B" of the CP code. Then all of the elements of group 2 simultaneously transmit codeword "A" and then codeword "B", and so on. The effect is to produce the spatial-temporal ground coverage shown below (Fig 25). The effective dwell time for each pixel is now

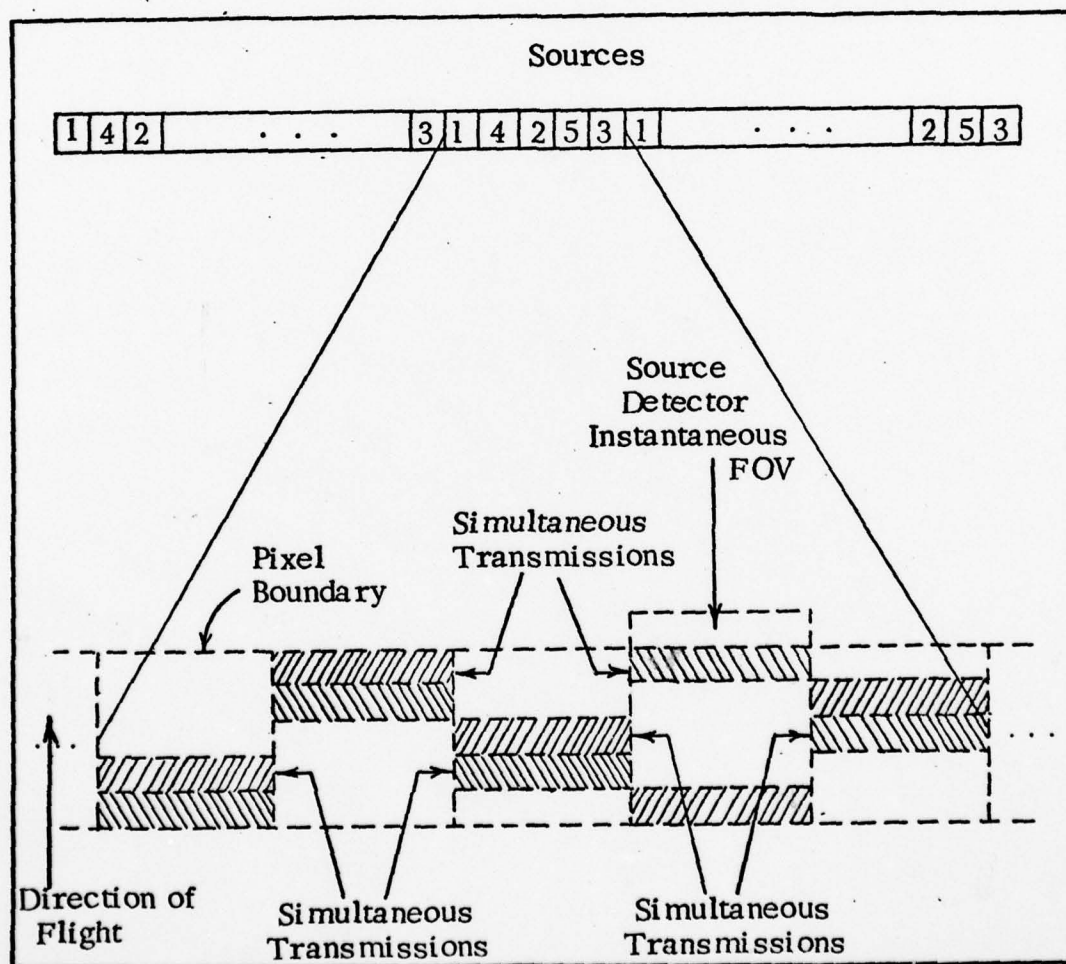


Fig 25. q-Staring Source-Detector Pairs, Spatially and Temporally Modulated

$2q\tau_d/5$, and the range and the reflectance mean square errors are given by

$$\sigma_r^2 \geq \frac{5}{2q} \cdot \frac{c^2 \lambda_n t_o}{8\rho^2 \beta^2 P_d^2 p} \quad (107)$$

$$\sigma_\rho^2 \geq \frac{5}{2q} \cdot \frac{4\lambda_n}{\beta^2 P_d^2 \tau_d} \quad (108)$$

and the maximum unambiguous range is given by

$$R_{amb} = \frac{qc\tau_d}{5} \quad (109)$$

This particular method of spatial coding into the q source-detector pairs results in 2.5 times degradation of both performance bounds and the ambiguous range when compared to the previous coding scheme.

Other configurations with more than five different element groups may be arrived at. Also if peak power limited output restraint is dropped and rms output is the same regardless of the duty cycle - then performance is the same as the previous case.

N Overlapping Sources, Pulse Code Modulation

The final spatial-temporal coding scheme to be discussed in the chapter considers the spatial combination of N sources by overlapping the N transmitted laser beams (Fig 26). No attempt is made to tightly collimate the beams. Instead, they are allowed to diverge rather broadly to

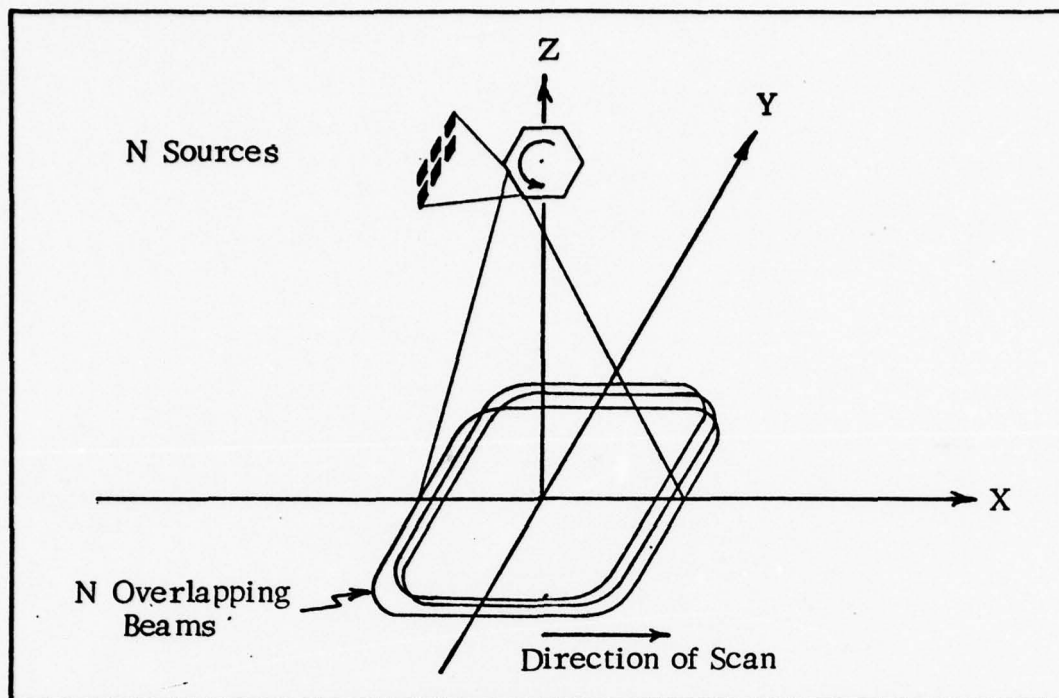


Fig 26. N Overlapping Transmitted Laser Beams

form a large "spotlight" type of "footprint" on the ground. Except at the edges, the average radiant emittance (watt/m^2) per pixel for such a spatial distribution is N times that for a single source line scan system. An array of N spatially orthogonal detectors are used to partition the large "footprint" into an array of N pixels (Fig 27). The "footprint" and N detectors FOVs may be scanned together, and all N of the sources may be temporally modulated simultaneously with the same pulse code. So long as the output of the detectors are combined so that the differences in radiant emittance per pixel and detector responsivities are averaged out, and not too much energy overfills the FOV of the N receivers, the performance can be shown to be exactly that of the other spatial-temporal coding combinations which used pulse code modulation. The slow scan $m \times n$ array receiver configuration is the simplest to implement. However, a fast scanning

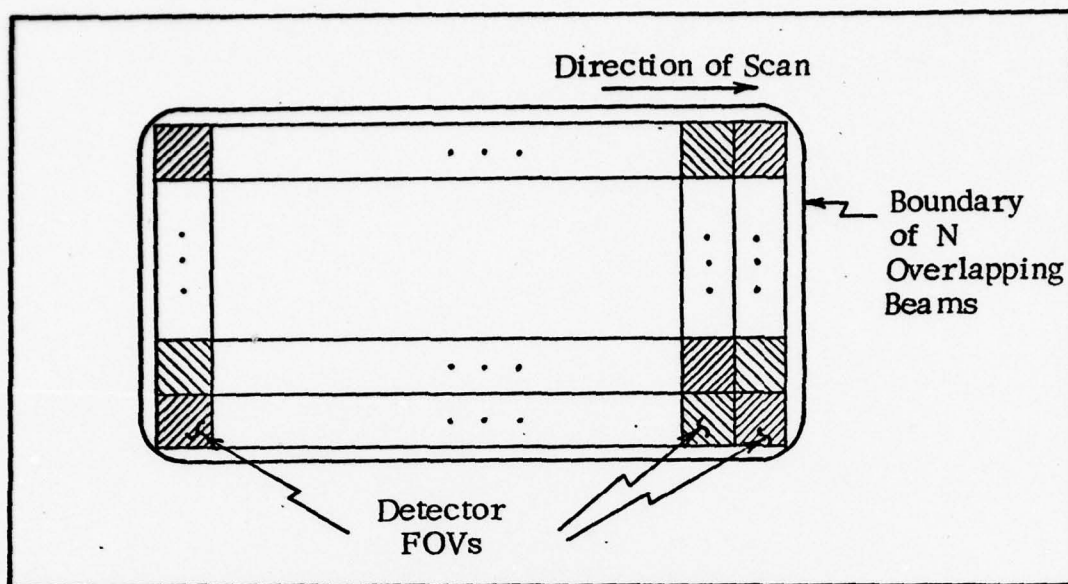


Fig 27. "Footprint" of N-Overlapping Beams Partitioned By N-Detector FOVs.

$m \times n$ array receiver which scans each line m times and uses delay lines to sum the $m \times n$ returns from each pixel will give the most uniform reflectance performance. The expressions for the range and the reflectance variances are given by Eqs (80) and (72) and the unambiguous range is given by

$$R_{amb} = \frac{N}{m} \frac{c \tau_d}{2} \quad (110)$$

where τ_d is the dwell time (codeword length) of each detector. The advantage of such an illumination scheme is that the requirements on the transmitter optics (usually diffraction limited) are greatly relaxed, and the differences in all the transmitter-powers and m of the photodetector responsivities are averaged out. Also, the number of transmitting laser diodes is arbitrary and need not be matched to the number of photodetectors used to partition the receiver FOV. The number of sources could, theoretically, be several times that of the detectors. However, in order to make systems comparisons easier, the number of sources will be limited to N for this analysis.

IV. Comparisons of the Various Spatial -Temporal Coding Combinations

The performance of the various spatial-temporal coding combinations developed in Chapter III will be compared in this chapter. The basis of comparison to be used will be that of the range and the reflectance estimation performance of the coding schemes. Comparisons will be made by relating the rms (standard deviation) of the range and the reflectance errors for each scheme. In addition, the maximum unambiguous range and the ease of implementation of the systems will be compared. Throughout all of the comparisons, it will be assumed that the values of the laser output power P_t and the photodetector responsivity $\beta = \eta/hf_0$ for each of the N laser transmitter-photodetector pairs are identical from pair-to-pair and coding-scheme to coding-scheme. It will also be assumed that the GaAs laser diodes are peak power limited and that the system modulation bandwidth is limited by the high frequency response of the laser diode or the photodetector, whichever is smaller.

In order to simplify the comparisons, the various spatial-temporal combinations presented in Chapter III will be divided into the three following classes: (1) Scanning configurations using pulse code modulation (PCM), (2) Scanning configurations using sinusoidal modulations, and (3) Non-scanning or staring configurations. Comparisons will be made within each class to determine the coding scheme with the best performance. The

resulting systems, one or two from each class, will then be compared. Also, since it was shown in Chapter III that there is no advantage to employing "Hybrid Spatial and Temporal Coding", it will not be included in the following comparisons.

It should be noted that the range performance will be the primary criterion for determining one system over another. As was shown by Eq (39), the reflectance performance depends only upon the postdetection signal energy and will be identical for all systems given the same total energy transmitted per pixel. It can also be shown that the range performance of a system will degrade faster than the reflectance performance as the signal-to-noise ratio (SNR) is decreased. The range estimation is made using either a matched filter or a phase locked loop; and both require the signal-to-noise ratio to be above some threshold. However, the reflectance estimation is made by simply integrating the receiver output, and is possible at SNRs much lower than the threshold required for operation of the matched filter or PLL. Also, the reflectance data is of secondary importance to the pattern recognition algorithms which primarily require range contours (derived from range gating).

Comparisons of the Pulse Code Modulation Class

All of the scanning configurations that use pulse code modulation, "N Sources-Parallel/Series/Array/Overlapping Beams", have identical expressions for the range and the reflectance variances. Thus the rms

error expressions will also be identical. This is true, regardless of whether the PCM modulation is the result of direct modulation (via direct current modulation) or indirect modulation (via electro-optic or spatial modulation). The major differences between these scan configurations are the resulting maximum unambiguous range, the implementation complexities, and the number of averaged transmitter-receiver pair responses.

Maximum Unambiguous Range. The maximum unambiguous range depends upon the codeword length, or pixel dwell time, and thus is a function of the scan configuration. Comparing Eqs (82)-(83) yields

$$\begin{aligned}
 &R_{\text{amb-Slow Parallel Scan, PN Code}} \\
 &= NR_{\text{amb-Single Source Scanner, PCM}} \\
 &= NR_{\text{amb-Fast Parallel Scan, PCM}} \\
 &= 2R_{\text{amb-Slow Parallel Scan, CP}} \\
 &= \frac{N}{m} R_{\text{amb-Scanning Array, PCM}} \\
 &= \frac{N}{m} R_{\text{amb-Overlapping Beams, PCM}} \quad (III)
 \end{aligned}$$

Thus the slow parallel scan is capable of the largest unambiguous range estimate. However, it should be noted that for a single source scanner with $\tau_d = 1 \mu\text{sec}$, the unambiguous range is 150 meters (490 feet), which should be adequate for providing target cues with a downward looking system. Therefore, all of the systems using pulse code modulation should provide adequate maximum unambiguous ranges for downward looking

systems. If the laser line scanner is to be used in a forward looking configuration where long slant ranges are involved, then longer unambiguous ranges may be desirable and the slow parallel or array scanning configuration might be more desirable. Otherwise, maximum unambiguous range is not a key parameter to be used in recommending one of the above pulse code modulation systems over another.

Implementation Complexity. The complexity of the transmitter, scanner, and the receiver all depend upon the scan configuration. The same linear array of N GaAs laser diodes is required for all of the parallel scan cases and the serial scan case, and thus will be equally hard to implement in each case, whether using a single substrate or N separate diodes. The $m \times n$ array required for the scanning array probably cannot be implemented on a single substrate, and would be several orders of magnitude more difficult to implement with individual diodes. As mentioned in Chapter III, the optics may be easier to implement for the Overlapping Beam Scan configuration than for the other scan configurations. For the remaining configurations, the optics are probably of the same degree of complexity from case-to-case. The dimensions of the rotating prism scanner might be changed, and the rotation rate might be reduced for the slow parallel and array scan cases, but otherwise the same degree of complexity is required for each of the scan configurations considered.

The most pronounced differences in implementation difficulty from one scan configuration to another occurs in the receiver. All of the

receivers for the scan configurations above require N photodetectors, either in a linear array, or in an $m \times n$ array. These type detectors are available and pose no major problems other than the non-uniformity of responsivity from detector-to-detector which occurs in both the linear or rectangular arrays. Reviewing the analysis results of Chapter III reveals that the Slow Parallel Scan case has the simplest implementation; it requires no delays or complicated switching network. The Series Scan case was slightly more complicated, requiring one delay line summer. The complexity increases in order with the Array Scan and Overlapping Beams, Fast Parallel Scans, and Slow Parallel Scan-CP Code; requiring m , q , and $qN/2$ delay lines summers, respectively. Hence the Slow Parallel Scan and the Serial Scan are perhaps the easiest scan configurations to implement when using pulse code temporal modulation. The relaxation of the optics complexities for the Overlapping Beams configuration may overcome the additional required receiver complexities (m delay lines) for the scan system.

Other Considerations. The various pulse code modulated scan configurations may be compared in several other respects, such as the degree of raster skew from the perpendicular to the aircraft ground track, and the number of averaged transmitter-receiver pair responsivities. In general, the faster the scan rate, the smaller the skew angle will be, and visa-versa. Therefore, since the two Fast Parallel Scanners and the Series Scanner sweep at the same rate as the Single Source System, they

will have identical skew angles. The Array Scan and Overlapping Beams configurations are scanned at $1/m$ times the rate of the single source, and thus have larger skew angles. The Slow Parallel Scan case is swept at $1/N$ times the single source sweep rate; and therefore, has the largest skew angle.

As was pointed out in Chapter III, the Series Scanner and the two Fast Parallel Scanners average out any differences in the N transmitter-receiver responsivities, thereby ensuring constant reflectance estimation performance from pixel-to-pixel. The Array Scanner and Overlapping Beams Scanner only average n of the receiver outputs, thereby allowing slightly different reflectance estimation performances between the n lines of each scan. The Slow Parallel Scanner does not average the outputs of any receivers, and thus allows for even greater reflectance estimation performance from line-to-line of the scan. It should be pointed out that the range estimates are the primary data required for target cueing, and the reflectance estimates are secondary data. Thus the loss of system performance due to non-uniformity of reflectance estimation performance depends upon the degree to which the pattern recognition algorithms require uniform reflectance estimation performance, and may not be too severe for the differences referred to here.

It follows from the previous discussion that the Series Scanner has the best overall PCM coded Scanner Characteristics. It has the same range and reflectance performance as the other configurations, has the

AD-A053 351

AIR FORCE INST OF TECH WRIGHT-PATTERSON AFB OHIO SCH--ETC F/G 20/5
SPATIAL AND TEMPORAL CODING OF GAAS LASERS FOR A LASER LINE SCA--ETC(U)
DEC 77 R S SHINKLE

UNCLASSIFIED

AFIT/GE0/EE/77-5

NL

2 of 2
AD
A053351



END
DATE
FILMED
6-78
DDC

smallest possible raster line skew angle, has uniform reflectance performance from line-to-line, and requires only one delay line summer. It is also the simplest method of implementing the linear CP code modulation, which has the most desirable autocorrelation properties. The preceding comparisons are summarized in Table I.

Comparisons of the Sinusoidal Modulation Class

The three spatial-temporal coding combinations in the sinusoid modulation class, "N Sources in Parallel-Sinusoidal Modulation/Multiple Sinusoidal Modulation/OOK Sinusoidal Modulation", will now be compared with each other.

Range and Reflectance Performance. The range performance of the three systems were compared in Chapter III and the standard deviation (rms) of the range error σ_r of the systems were shown to be related by

$$\begin{aligned}\sigma_{r-S} &= \frac{1}{2} \sigma_{r-M} \\ &= \frac{1}{\sqrt{2}} \sigma_{r-OOK}\end{aligned}\tag{112}$$

where the subscripts S, M, and OOK denote Single, Multiple and On-Off-Keyed Sinusoidal Modulation, respectively. The reflectance performances were also compared, yielding

$$\begin{aligned}\sigma_{p-S} &= 1.1 \sigma_{p-M} \\ &= \sqrt{2} \sigma_{p-OOK}\end{aligned}\tag{113}$$

where σ_p is the reflectance error standard deviation. Thus the best

Table I

Comparison of PCM Scan Characteristics

Configuration	Range Ambiguity Interval	Number Delay Lines Required	Number Channels Averaged/Pixel	Complexity of Optics
Slow Parallel Scan, PCM	Largest	None	0	
Fast Parallel Scan, PCM	↑	q	N	
Slow Parallel Scan, CP Code	Smallest	$qN/2$	2	
Fast Parallel Scan, CP Code	↓	q	N	
Serial Scan		1	N	
Array Scan	Intermediate	m	n	Most Severe
Overlapping Beams	Intermediate	m	n	Least Severe

possible range and reflectance performance is achieved by the Single Sinusoidal Modulation System. The next best range performance is obtained by the OOK Sinusoidal Modulation System. The reflectance performance for the OOK Sinusoid case is only 29% worse than that of the Multiple Sinusoid case. Since the reflectance data is of secondary importance, the OOK Sinusoidal Modulation system is the second best sinusoidal modulation technique for estimating range and performance.

Maximum Unambiguous Range . The maximum unambiguous range for the three sinusoidal modulation techniques were given by

$$R_{\text{amb-S}} = \frac{c}{2f_m} \quad (74)$$

$$R_{\text{amb-M}} = \frac{c}{2f_m} \quad (90)$$

$$R_{\text{amb-OOK}} = \frac{Nc\tau_d}{2} \quad (82)$$

For parameters that might be typical of laser line scan systems, assume $f_m = 100$ MHz, $f = 1$ MHz, $N = 10$, and $\tau_d = 1 \mu\text{sec}$. For these parameters, Eqs (74), (90), and (82) yield unambiguous ranges of 1.5 meters, 150 meters, and 1500 meters respectively. Thus the later two modulation techniques give orders of magnitude better unambiguous ranges than the Single Sinusoid case, with the OOK Sinusoidal Modulation case yielding the best results.

Implementation Complexity. All three of the sinusoidal modulation techniques use the "N Sources in Parallel" scan type and are of equal complexity. The modulation of the drive current of the laser diode transmitters is of equal complexity for the Multiple and OOK Sinusoidal Modulation cases and is only marginally more complicated than that of the Single Sinusoidal Modulation case. The receiver configuration complexity increases in order with the Single, Multiple, and OOK Sinusoidal Modulation Techniques. However, the increased complexity of the OOK Sinusoid case is not that severe compared to the Multiple Sinusoid case and is certainly worth the large increase in unambiguous range with only a $\sqrt{2}$ reduction in performance compared to the Single Sinusoid case. Note that since all three of these sinusoidal modulation techniques use the same type of scan, they will have identical raster line skew angles and reflectance performance behavior from line to line.

Comparisons of the Non-Scanning Class

The two non-scanning configurations, "q-Staring Sources and Detectors - Pulse Code Modulation/Spatial and Temporal Modulation" may be compared by inspection. The two schemes are exactly the same except the latter uses spatial coding to overcome optics deficiencies in order to ensure strict temporal orthogonality between adjacent channels. This reduces the effective dwell time, and therefore, the efficiency of the pulse code modulation, by a factor of 2/5. Hence the standard deviation of the

range and the reflectance errors increase by a factor of 1.58 and the unambiguous range is decreased by a factor of 1.25 compared to the staring scheme which does not employ spatial coding. Thus the non-spatial-temporal coded case has the best performance. Note that the use of the spatial coding merely reduces the temporal cross talk occurring when the illumination from one channel lies in the field-of-view of another channel. It does not reduce inter-pixel spatial cross talk due to the illumination of a given channel overspilling the pixel, thereby causing "noisy" range and reflectance estimates.

Comparison of PCM and Sinusoidal Modulations

Range and Reflectance Performance. The next comparison is between the N Sources in Series, Pulse Code Modulation system and the N-Sources in Parallel, Single Sinusoidal Modulation System. The range performance of these two systems can be compared by algebraically combining Eqs (80) and (86), resulting in

$$\sigma_{r-PCM} = \frac{\pi}{2} t_0 f_m \sigma_{r-S} \quad (114)$$

where σ_{r-PCM} and σ_{r-S} are the standard deviations of the range error of the PCM system and the Single Sinusoid system, respectively. Likewise, the reflectance performance can be compared by combining Eqs (81) and (87), yielding

$$\sigma_{\rho-PCM} = 0.87 \sigma_{\rho-S} \quad (115)$$

where $\sigma_{\rho\text{-PCM}}$ and $\sigma_{\rho\text{-S}}$ are the standard deviations of the reflectance error for the PCM systems and the Single Sinusoid System, respectively. Thus the reflectance performance of the PCM system is always better than that of the Single Sinusoid system. From Eq (114), it is easily shown that in order for the PCM system range performance to be greater than that of the Single Sinusoid system, the chip duration t_0 must be such that

$$t_0 \leq \frac{0.64}{f_m} = 0.64 T_m \quad (116)$$

where T_m is the period of the modulation sinusoid. If f_m is the upper limit of the frequency response of the laser diode, then the only way the PCM system can be made to outperform the single sinusoid system is to use indirect (electro-optic or spatial) modulation. If f_m is the upper limit of the frequency response of the photodetector, then it is impossible for the PCM system to outperform the Single Sinusoid System in range estimation.

Maximum Unambiguous Range. The maximum unambiguous range for the two systems are given by Eqs (83) and (74), and are

$$R_{\text{amb-PCM}} = \frac{c p t_0}{2} \quad (83)$$

$$R_{\text{amb-S}} = \frac{c}{2 f_m} \quad (74)$$

For typical system parameters of $p t_0 = \tau_d = 1 \mu\text{sec}$ and $f_m = 100 \text{ MHz}$, the unambiguous ranges for the two expressions above are 150 meters and 1.5 meters, respectively. Thus it is seen that PCM system has a superior unambiguous range resolution capability.

From the above discussion, it can be concluded that the Single Sinusoid system is superior if the short range ambiguity is acceptable. If longer unambiguous ranges are required, one must pick an acceptable range ambiguity and then use Eq (74) to calculate the required f_m . The calculated f_m , and the smallest chips width to which the overall system is capable of responding to must then be used in Eqs (80) and (86) to determine which system has the best performance for the required unambiguous range. This comparison can be simplified by graphical methods. Solving Eq (74) for f_m and substituting into Eq (114) yields

$$\sigma_{r-PCM} = \frac{\pi c t_0}{4 R_{amb}} \sigma_{r-s} \quad (117)$$

Solving Eq (117) for R_{amb} and setting $\sigma_{r-PCM} = \sigma_{r-s}$ results in

$$R_{amb} = \frac{\pi c}{4} t_0 \quad (118)$$

which may be plotted as shown below (Fig 28). Now if the intersection of the desired unambiguous range and available state-of-the-art t_0 lies above the $\pi c t_0/4$ line, the PCM system will give the best performance; if the intersection falls below the line, then the Single Sinusoid system is the best choice.

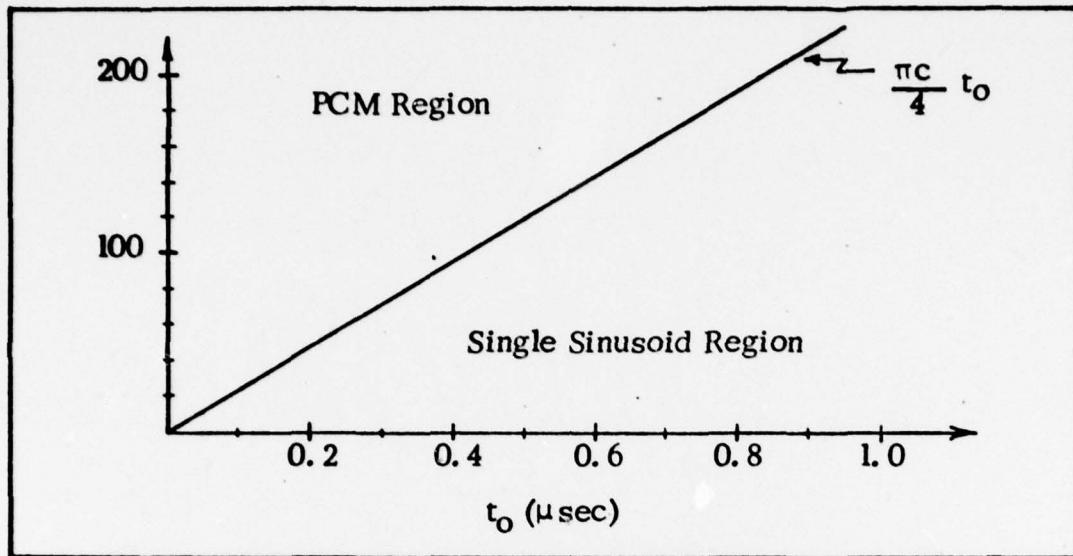


Fig 28. Graph of $R_{amb} = \frac{\pi c}{4} t_0; \left(\frac{\sigma_{r-s}}{\sigma_{r-PCM}} = 1 \right)$

Comparison of PCM and OOK Sinusoidal Modulations

Range and Reflectance Performance. The next comparison is between the N Sources in Series, Pulse Code Modulation system and the N Sources in Parallel, OOK Sinusoidal Modulation system. The respective range performance may be compared by combining Eqs (80) and (97), yielding

$$\sigma_{r-PCM} = \frac{\pi}{2\sqrt{2}} f_m t_0 \sigma_{r-OOK} \quad (119)$$

where σ_{r-PCM} and σ_{r-OOK} range error standard deviations for the PCM and OOK Sinusoidal Modulated systems, respectively. Likewise, the reflectance performances may be compared by combining Eqs (81) and (98), giving

$$\sigma_{p-PCM} = 0.61 \sigma_{p-OOK} \quad (120)$$

where $\sigma_{\rho\text{-PCM}}$ and $\sigma_{\rho\text{-OOK}}$ are the reflectance error standard deviations for the PCM and OOK sinusoidal modulated systems, respectively. Thus the PCM system will always have the better reflectance performance. However, the PCM system will have the better range performance only if

$$t_o \leq \frac{0.90}{f_m} = 0.9 T_m \quad (121)$$

As stated earlier, if the frequency response of the system is limited by the laser diode, then indirect modulation must be used in order for the PCM system to have better range performance than the OOK Sinusoid system. If the system frequency response is limited by the detector, then the OOK Sinusoid system will always have the better performance.

Maximum Unambiguous Range . The maximum unambiguous range of the N Sources in Series, PCM Modulation system and that of the N Sources in Parallel, OOK Sinusoidal Modulation system may be compared by combining Eqs (82) and (83), yielding

$$R_{\text{amb-OOK}} = N R_{\text{amb-PCM}} \quad (122)$$

Note that the restriction on t_o given by Eq (102) must be met in order for Eq (122) to be valid. So long as that restriction is satisfied, there is no advantage to using the PCM system to resolve range. Thus, based on the above analysis of all the scanning systems using N sources, the OOK Sinusoidal Modulation system has the best range performance if large range ambiguity is required. If large range ambiguities are not required,

then the Single Sinusoidal Modulation system has the best range performance.

Implementation Complexity. Both the Series Scan, PCM system and the Parallel Scan, OOK Sinusoidal Modulation system use the same linear array of laser diodes, the same optics and except for perhaps minor changes in dimensions or rotational rate, the same scanner. The receiver-processor for the OOK Sinusoid system is more complicated than that of the PCM receiver due to the number of PLL, mixers, and filters required. However, it is much more practical to realize than some of the Fast Parallel Scan system described earlier, and is certainly not unreasonable. Sinusoids are also easier to generate than nanosecond switching networks and delays.

Other Considerations. The PCM system above employs the serial scanner and thus has uniform reflectance estimation performance from line-to-line as well as a small raster line skew angle. The OOK Sinusoidal Modulation system, on the other hand, employs the parallel scanner. Thus the OOK Sinusoidal Modulation system does not average any of the receiver output; and therefore, may not necessarily exhibit uniform reflectance estimation performance from line-to-line of the raster scan. However, depending upon the requirements of the pattern recognition algorithm, this may or may not be a serious problem. The OOK Sinusoidal Modulation system also has a larger raster line skew angle than the PCM system. However, this is not a major concern since the raster lines may be de-skewed by the pattern recognition processor.

It is important that one other point be recognized here. The above analysis comparing the PCM Serial Scan system to the OOK Sinusoidal Modulation system could be generalized to include the other scan configurations that employ PCM with few changes. However, if the Overlapping Beams scan configuration is not restricted to N sources, then the general comparisons above will not apply. Through the brute force technique of adding more sources; and consequently, more energy per pixel; the frequency response deficiency of the PCM coding scheme can be overcome. Thus, the Overlapping Beams, PCM coding scheme can be made to outperform the Single or the OOK Sinusoidal Modulation coding schemes. This system also has the advantages of averaging N receiver outputs per scan line, a reduced raster line skew angle and possibly simpler transmitter optics.

Comparison of q-PCM Channels and N-OOK Sinusoidal Modulation Channels

Range and Reflectance Performance. The final two systems to be compared are the N Sources in Parallel, OOK Sinusoidal Modulation system and the q-Staring Sources and Detectors, PCM system. The range performance of the two systems may be compared by combining Eqs (97) and (103), resulting in

$$\sigma_{r-N-OOK} = \frac{0.9}{f_{m t_0}} \sqrt{\frac{q}{N}} \cdot \sigma_{r-q-PCM} \quad (123)$$

where $\sigma_{r-N-OOK}$ and $\sigma_{r-q-PCM}$ are the rms range estimation errors for the N-OOK source system and the q-PCM source system, respectively. The reflectance performance of the two systems may be compared by combining Eqs (98) and (104), yielding

$$\sigma_{p-N-OOK} = 1.15 \sqrt{\frac{q}{N}} \cdot \sigma_{p-q-PCM} \quad (124)$$

where $\sigma_{p-N-OOK}$ and $\sigma_{p-q-PCM}$ are the rms reflectance estimation errors for the N-OOK source system and the q-PCM source system, respectively. The above results are hard to interpret because of the many independent variables. However, the range estimation performance of the N-source system can only exceed that of the q-source system if

$$\frac{0.9}{f_m t_0} \sqrt{\frac{q}{N}} < 1 \quad (125)$$

Solving Eq (125) for N gives

$$N > \left(\frac{0.9}{f_m t_0} \right)^2 q \quad (126)$$

Two examples will give a better insight as to the relationship between $\sigma_{r-N-OOK}$ and $\sigma_{r-q-PCM}$. If $q = 1000$, and $t_0 = 5/f_m$, then $N > 33$ in order for the N-OOK source system to have the smaller rms range error. If $q = 10,000$ and $t_0 = 10/f_m$, then N need only be 81 to outperform the 10,000 element staring system. This indicates that the improvement in the range performance, which is proportional to the square root of the number of sources, is not worth the additional complexity

involved for the q-source staring system. These results are general enough that they can be expanded to the Overlapping Beams, PCM case also, where the number of overlapping sources is allowed to be q, $q > N$. Thus, if a laser line scanner is required to have a long unambiguous range, then the N Sources in Parallel, OOK Sinusoidal Modulation combination of spatial and temporal coding will yield the best overall range and reflectance estimation performance. The comparisons results of this chapter are summarized in Table II.

Table II
Spatial-Temporal Systems Characteristics

System	σ_r	σ_ρ	Range Ambiguity Interval	Optics Complexity
Serial Scan, PCM	$\frac{\pi}{2} f_m t_o \sigma_{r-s}$	$\sigma_{\rho-PCM}$	$c\tau_d/2$	
Overlapping Beams, PCM	$\frac{\pi}{2} f_m t_o \sigma_{r-S}$	$\sigma_{\rho-PCM}$	$c\tau_d/2$	Least
Parallel Scan, Single Sinusoidal Modulation	σ_{r-S}	$1.15 \sigma_{\rho-PCM}$	$c/2f_m$	Severe
Parallel Scan, OOK Sinusoidal Modulation	$\sqrt{2} \sigma_{r-s}$	$1.63 \sigma_{\rho-PCM}$	$c\tau_d/2$	

As an example of the range performance which might be expected with a multiple source GaAs laser line scan system, assume the following system parameters: $N = 10$, $P_t = 1$ watt, $E_{s,0.85\mu m} = 0.07$ watts/cm²- μm , $\rho = 0.1$, $\theta = 0^\circ$, $t_r = t_t \approx 1$, $A_r = 100$ cm², $A_f = 900$ cm² (~ 1 ft x 1ft), $r = 2.5 \times 10^4$ cm (~ 820 ft), $\Delta\lambda = 0.01$ μm , $f_m = 100$ MHz, and $\tau_d = 1$ μsec .

Using Eq (77), (78) and (97), recognizing that $\lambda_n = \beta P_b$, the rms range error for the OOK Sinusoidal Modulation system is $\sigma_{r\text{-OOK}} = 2.3 \times 10^{-1} \text{cm}$, certainly good enough target for cueing. Note that this is the best performance possible, theoretically. Actual attainable rms error may be larger. Also, this example was calculated assuming no losses due to the atmosphere or optics, and neglected noise due to atmospheric backscatter. For operation in fog or haze the performance would degrade appreciably. Thus the use of several sources for clear weather operation may seem like overkill, but may be quite necessary of inclement weather operation. Also, note that the rms range error varies as f_m^{-1} and as $(NP_d)^{-\frac{1}{2}}$. Thus it is more important to use sources with good high frequency response than with high output powers, and the number of sources N required will depend upon f_m , P_d , and the performance required.

Comparisons Results: rms Power Limited Sources

All of the preceding analysis assumed the GaAs laser diodes were peak power limited. If this assumption were removed, the above results would change only slightly. Since Eq (39) indicates that the reflectance performance depends only upon the post detection signal energy, removal of the peak power limited restriction means that all of the spatial-temporal coding combinations will have identical reflectance performances. As for the range performance, removal of the restriction enables the performance of the q-Staring Sources and Detectors, Spatial and Temporal Modulation

case to equal that of the q-Staring Sources and Detectors, PCM case. It also allows the reflectance performance of all of the sinusoidal cases to be equal. However, it can be shown that if Eqs (80) and (86) are normalized by E_{s-PCM} and $E_{s-Sinusoid}$, respectively, and the algebraically combined, the result is

$$\sigma_{r-PCM} = \frac{\pi}{\sqrt{2}} f_m t_o \sigma_{r-s} \quad (127)$$

Therefore, it is required that

$$t_o \leq \frac{\sqrt{2}}{\pi} T_m \quad (128)$$

in order for the PCM system to outperform the sinusoidal system. Therefore, even if the peak power limited restriction is removed, the best range performance is still achieved by using sinusoidal modulation or OOK sinusoidal modulation.

V. Conclusions and Recommendations

This Chapter contains the general conclusions based upon the analysis and comparisons of the previous chapters, and lists several recommendations for further investigation.

Conclusions

The basic purpose of this study was to find the combination of scan configuration, for N GaAs laser diode sources, and intensity modulation temporal coding which would produce optimum range and reflectance estimation performance. Toward this end, the statistical additive noise model for a direct (optical intensity) detector was developed. Estimation theory, based upon the conditional Poisson statistics of the detector, was used to develop the joint maximum-likelihood (ML) estimator (mathematical model) for both range and reflectance. The realization of the joint estimator was a correlator which required the reflectance estimate times a replica of the transmitted signal (delayed by the time estimate) for an input. The joint estimator could not be easily realized. However, it was shown that a realization of the range estimator is a matched filter, and a suboptimum realization of the reflectance estimator is the measurement of the detected signal energy, given the range estimate. The Cramer-Rao lower bound was calculated for both range and reflectance estimates. The variance of the range error is inversely proportional to the mean square bandwidth of the modulating signal, and the variances of both the range and the reflectance

errors are inversely proportional to the detected signal energy. Various combinations of spatial and temporal coding of the N laser sources to separate the return signal energy from each ground resolution cell while increasing the returned energy per cell were evaluated. This was done by analyzing a large variety of spatial-temporal and hybrid spatial-temporal coding schemes and then comparing the performance results. Unfortunately, one technique is not always superior; the best scanning-coding combination to use depends upon the requirements of the pattern recognition algorithm. Nonetheless, several general conclusions may be made and will be discussed below.

The suboptimum matched filter/peak detector realization of the joint estimator is suboptimum because the round trip delay estimate is required in order to obtain the reflectance estimate. Therefore, the reflectance measurement is dependent upon the delay measurement. However, this appears to be the best possible processor configuration which can be constructed using current technology. The performance predicted by the Cramer Rao lower bound on the mean square estimation error is the smallest error limit theoretically possible. Regardless of the processor used, a performance better than the Cramer Rao lower bound can not be achieved. In practice, this lower bound may not be reached easily. Yet the Cramer Rao lower performance bound serves as a standard, or bench mark against which the performance of real systems may be compared. And

since the performance lower bounds calculated for the systems suggested in this thesis are well within an acceptable range, it is practical to try to build a laser line scan sensor using N GaAs semiconductor laser sources.

If the main goal of the laser line scan system design is to achieve the smallest possible range and reflectance errors, and if the short ambiguity interval and lack of uniform reflectance estimation performance from line-to-line is not a problem, then the parallel scan configuration (Fig 12, page 43) using sinusoidal intensity modulation is the best choice. However, if longer ambiguity intervals are required, then the same parallel scan configuration using On-Off-Keyed sinusoidal modulation appears to be the preferred technique. If in addition to long ambiguity intervals, uniform reflectance estimation performance from line-to-line is required, then either the pulse code modulated serial scan configuration (Fig 15, page 50) or the pulse code modulated overlapping beams scan configuration (Fig 26, page 72) may be used. In the latter case, the overlapping beams configuration may have slight reflectance performance variations from line-to-line, but may employ simpler transmitter optics. All of the other techniques require that the N individual transmitter fields-of-view do not overlap, i. e. , are spatially orthogonal, and all of the above techniques require the receiver fields-of-view to be spatially orthogonal. It is concluded that the most cost effective system with the best overall range, reflectance, and maximum unambiguous range characteristics available

using existing technology is the N Sources in Parallel, OOK Sinusoidal Modulation scheme. The sinusoidal modulation frequency f_m should be as high as possible, and will be limited by the upper frequency response of the source or the photodetector, whichever is lower. Narrow (fast risetime) optical pulses are not required, thus wide bandwidths are not required. The detector need only be fast; it does not need to have DC to RF frequency response. High peak power GaAs laser diodes are not essential, but high peak powers combined with high frequency responses ensure better performance in inclement weather and reduces the number of sources required.

Recommendations

Based on the conclusions above, the first recommendation for further work in this area is for a detailed study to examine existing or proposed cueing algorithms in order to determine what ambiguous range interval and reflectance performance criteria are required. This would then be used to determine which of the four techniques above should be emphasized the most in future research.

Another area requiring further investigation is that of spatial filtering. The scanning process was modeled as if the illuminating beam moves discretely from pixel to pixel with no smearing due to the beam movements or forward motion of the aircraft. There are some indications that the spatial filtering may be significant; therefore, the area warrants additional investigation.

In order to limit the scope of the study, the only pulse modulation codes considered were Barker codes, pseudo-noise (PN) codes, and Totally Orthogonal Complimentary Pair (CP) codes. There are other coding schemes with long codes and bi-level autocorrelation. This is an area which deserves more attention.

This analysis assumed that the Fields-of-View (FOV) of the transmitter optics and the receiver optics could be matched, and could be made spatially orthogonal to adjacent transmitter-receiver pair FOV. Since the GaAs laser diode output beam has a rather large divergence, this may not be true. Therefore, the feasibility of implementing the optics for each of the recommended scan techniques above should be evaluated. Also, the problem of summing the outputs of N laser diodes into a single narrow beam deserves further investigation. Further study is needed to determine the central beam characteristics of GaAs source and how to control the beam characteristics using both diode fabrication and optics.

The final recommendation is for further work in component technology. A concentrated effort to develop linear arrays of laser diodes, and of photodetectors, with uniform performance from element to element is desirable. An initial goal of five or ten GaAs laser diodes in a linear array might be reasonable.

Bibliography

1. Chapuran, Robert C. An Analysis of Modulation Techniques for the Simultaneous Measurement of Range and Reflectance Information by an Airborne Laser Scanner. Unpublished thesis. Wright-Patterson Air Force Base, Ohio: Air Force Institute of Technology, December 1976.
2. Perkin-Elmer Corporation. Gallium Arsenide (GaAs) Diode Laser, RF Experiment Results. Report No. 13170. Norwalk, Connecticut: Perkin-Elmer Corporation, October 1976.
3. Hoversten, E. V. "Optical Communication Theory" in Laser Handbook edited by F. T. Arecchi and E. O. Schulz-DuBois. Amsterdam, The Netherlands: North-Holland, 1972.
4. Pratt, William K. Laser Communication Systems. New York: John Wiley & Sons, Inc., 1969.
5. Gagliardi, Robert M. and Sherman Karp. Optical Communications. New York: John Wiley & Sons, Inc., 1976.
6. Van Trees, Harry L. Detection, Estimation, and Modulation Theory, Part I: Detection, Estimation, and Linear Modulation Theory. New York: John Wiley & Sons, Inc., 1968.
7. Snyder, Donald L. Random Point Processes. New York: John Wiley & Sons, Inc., 1975.
8. Ziemer, R. E. and W. H. Tranter. Principles of Communications. Boston: Houghton Mifflin Company, 1976.
9. Van Trees, Harry L. Detection, Estimation, and Modulation Theory, Part III: Radar-Sonar Signal Processing and Gaussian Signals in Noise. New York: John Wiley & Sons, Inc., 1971.
10. Lindsey, William C. and Marvin K. Simon. Telecommunications Systems Engineering. Englewood Cliffs, New Jersey: Prentice-Hall, Inc., 1973.
11. French, Charles. Totally Orthogonal Complementary Binary Coded Sequences and Applications to Communications Systems. Unpublished Thesis. Monterey, California: Naval Post-graduate School, June 1971.

12. Seyrafi, Khalil, Editor. Engineering Design Handbook: Infrared Military Systems, Part I (Includes Change I, Dated 7 May 1973). U.S. Army Materiel Command, AMC Pamphlet No. 706-127, April 1971. (AD-763495).
13. Radio Corporation of America. Electro-Optics Handbook. Harrison, N.J.: Radio Corporation of America, 1968.
14. Skolnik, Merrill I. Introduction to Radar Systems. New York: McGraw-Hill Book Company, 1962.
15. Yariv, Amnon. Introduction to Optical Electronics (Second Edition). Chicago: Holt, Rinehart and Winston, 1976.
16. Teague, J.R. and L. B. Allen. Advanced Modulator II, Final Report, March - November 1973. Wright-Patterson Air Force Base: Air Force Avionics Laboratory, 16 May 1974. AFAL-TR-74-17 (AD 922519).

Appendix A

Additive Noise Model for Direct Detection

The purpose of this appendix is to develop the additive noise model for a direct detector shown in Chapter II (Fig 1). The total detector output current is

$$i_d(t) = i_s(t) + i_b(t) + i_D(t) + i_{Th}(t) \quad (129)$$

The mean of the filter output will be the expected value of $i_d(t)$ convolved with the impulse response of the filter. Therefore,

$$E[y(t)] = E[i_d(t)] * h(t) \quad (130)$$

In order to evaluate $E[i_d(t)]$, one may use the fact that

$$i(t) = q \frac{dN(t)}{dt} \quad (131)$$

where N is the total number of counts (detected photons) over the observation interval. Using Eq (131), one finds that in general (Ref 4: 258-260)

$$E[i(t)] = q\lambda(t) \quad (132)$$

and

$$R_i(t, t') = q^2 \lambda(t) \delta(t-t') + q^2 \lambda(t) \lambda(t') \quad (133)$$

Eq (132) and Eq (133) imply that the combination of dark current plus background noise $i_n(t) = i_b(t) + i_D(t)$ may be modeled as

$$E [i_n(t)] = q \lambda_n \quad (134)$$

$$R_{i_n}[t, t'] = q^2 \lambda_n^2 + q^2 \lambda_n \delta(t-t') \quad (135)$$

where $\lambda_n = \lambda_b + \lambda_D$. It was mentioned in Chapter II that the thermal noise has first and second moments

$$E [i_{Th}(t)] = 0 \quad (136)$$

and

$$R_{i_{Th}}[t, t'] = 2 \frac{KT}{R_e} \delta(t-t') \quad (137)$$

Using Eqs (130), (132), (133), (134), and (135), becomes

$$E [i_d(t)] = q \lambda_s(t) + q \lambda_n \quad (138)$$

Writing Eq (130) in integral form and substituting Eq (138) yields

$$E [y(t)] = \int_{-\infty}^{\infty} h(t-\alpha) q \{ \lambda_s(\alpha) + \lambda_n \} d\alpha \quad (139)$$

The autocorrelation of the filter output will be the autocorrelation of $i_d(t) * h(t)$ and may be expressed as

$$R_y(t, t') = \int_{-\infty}^{\infty} d\alpha \int_{-\infty}^{\infty} d\beta h(t-\alpha) h(t'-\beta) E [i_d(\alpha) i_d(\beta)] \quad (140)$$

Using $E [X] = E [X] E [Y]$ for X and Y statistically independent, and substituting Eq (129), and Eqs (131) thru (136) and rearranging gives

$$\begin{aligned} E [i_d(\alpha) i_d(\beta)] &= \{ q^2 [\lambda_s(\alpha) + \lambda_n] + 2 \frac{KT}{R_e} \} \delta(\alpha - \beta) \\ &+ q^2 \{ \lambda_s(\alpha) \lambda_s(\beta) + \lambda_n [\lambda_s(\alpha) + \lambda_s(\beta)] + \lambda_n^2 \} \end{aligned} \quad (141)$$

The covariance of the filter output is given by

$$C_y(t, t') = R_y(t, t') - E[y(t)] E[y(t')] \quad (142)$$

Substituting Eqs (138) thru (141) into Eq (142) and simplifying yields

$$C_y(t, t') = \int_{-\infty}^{\infty} d\alpha \int_{-\infty}^{\infty} d\beta \{ q^2 [\lambda_s(\alpha) + \lambda_n] + 2 \frac{KT}{R_e} \} \delta(\alpha - \beta) \quad (143)$$

Therefore, zero mean additive noise model may be represented by letting the input be $E[i_d(t)]$ and the additive noise be $n(t)$ with $R_n(t, t') = C_y(t, t')$. The schematic of the resulting noise model is shown in Chapter II (Fig 1).

VITA

Reese Stanley Shinkle was born on 11 October 1948 in Huntsville, Alabama. He graduated from high school in 1967, then attended Auburn University where he participated in the co-operative education program with NASA, George C. Marshall Space Flight Center, Huntsville, Alabama. While working for NASA, he worked with analog and digital signal processing for both communications and radar systems, GaAs laser range-finders, and fiber-optic data links. Upon graduation from Auburn University with the degree Bachelor of Electrical Engineering in December 1972, he received a commission in the USAF through the AFROTC program. His first assignment was to the 544th Aerospace Reconnaissance Wing, Headquarters, Strategic Air Command, Offutt AFB, Nebraska, where he served as an electronic intelligence and radar analyst. He entered the School of Engineering, Air Force Institute of Technology, in June 1976 and is presently pursuing a masters degree in the Electro-Optics program.

Permanent address: Route 1, Box 542
Huntsville, Alabama 35810

UNCLASSIFIED

SECURITY CLASSIFICATION OF THIS PAGE (When Data Entered)

REPORT DOCUMENTATION PAGE		READ INSTRUCTIONS BEFORE COMPLETING FORM
1. REPORT NUMBER GEO/EE/77-5	2. GOVT ACCESSION NO.	3. RECIPIENT'S CATALOG NUMBER
4. TITLE (and Subtitle) SPATIAL AND TEMPORAL CODING OF GaAs LASERS FOR A LASER LINE SCAN SENSOR		5. TYPE OF REPORT & PERIOD COVERED MS Thesis
7. AUTHOR(s) Reese S. Shinkle Captain, USAF		6. PERFORMING ORG. REPORT NUMBER
9. PERFORMING ORGANIZATION NAME AND ADDRESS Air Force Institute of Technology (AFIT-EN) Wright Patterson AFB, Ohio 45433		8. CONTRACT OR GRANT NUMBER(s)
11. CONTROLLING OFFICE NAME AND ADDRESS Electro-Optics and Reconnaissance Branch (AFAL-RWI) Air Force Avionics Laboratory Wright-Patterson AFB, Ohio 45433		10. PROGRAM ELEMENT, PROJECT, TASK AREA & WORK UNIT NUMBERS
14. MONITORING AGENCY NAME & ADDRESS (if different from Controlling Office)		12. REPORT DATE December 1977
		13. NUMBER OF PAGES 123
		15. SECURITY CLASS. (of this report) Unclassified
16. DISTRIBUTION STATEMENT (of this Report) Approved for public release; distribution unlimited.		15a. DECLASSIFICATION/DOWNGRADING SCHEDULE
17. DISTRIBUTION STATEMENT (of the abstract entered in Block 20, if different from Report)		
18. SUPPLEMENTARY NOTES Approved for public release; IAW AFR 190-17 <i>Jerome F. Guess</i> JEROME F. GUESS, Captain, USAF Director of Information		
19. KEY WORDS (Continue on reverse side if necessary and identify by block number) Target Cueing Active Line Scanner Terrain Mapping Range Measurement Laser Line Scanner Reflectance Measurement Laser Rangefinders Spatial and Temporal Coding		
20. ABSTRACT (Continue on reverse side if necessary and identify by block number) This paper establishes the coding combination of intensity modulation and scan pattern for N GaAs laser sources which results in the optimum measurement of range and reflectance via an active laser line scan sensor. Estimation theory, based upon quantum nature of the photodetector, is used to show that the optimum estimators for range and reflectance estimates are, respectively, a correlator or matched filter; and a measurement of the received signal energy, given the range estimate. It is shown that the root mean square (rms) range		

DD FORM 1 JAN 73 1473

EDITION OF 1 NOV 65 IS OBSOLETE

UNCLASSIFIED